Inorganic Chemistry

pubs.acs.org/IC Article

Stoichiometrically Controlled Assembly of Lanthanide Molecular Complexes of the Heteroditopic Divergent Ligand 4′-(4-Pyridyl)-2,2′:6′,2″-terpyridine *N*-Oxide in Hypodentate or Bridging Coordination Modes. Structural, Magnetic, and Photoluminescence Studies

Lorenzo Fioravanti, Luca Bellucci, Lidia Armelao, Gregorio Bottaro, Fabio Marchetti, Francesco Pineider, Giordano Poneti, Simona Samaritani, and Luca Labella*

Cite This: *Inorg. Chem.* 2022, 61, 265−278 Read Online

ACCESS | Metrics & More | Article Recommendations | Supporting Information

ABSTRACT: Mononuclear rare-earth tris-β-diketonato complexes RE(tta)$_3$dme [RE = Y (**1**), La (**2**), Dy (**3**), or Eu (**4**); Htta = 2-thenoylacetone; dme = 1,2-dimethoxyethane] react cleanly at room temperature in a 1:1 molar ratio with the heteroditopic divergent ligand 4′-(4-pyridyl)-2,2′:6′,2″-terpyridine *N*-oxide (pyterpyNO) to yield RE$_2$(tta)$_6$(pyterpyNO)$_n$, where n = 2 for RE = Y (**5**), Dy (**6**), or Eu (**7**) and n = 3 for RE = La (**8**). The crystal structure of **5** revealed a dinuclear compound with two pyterpyNO's bridging through the oxygen atom in a hypodentate mode leaving the terpyridine moieties uncoordinated. Using a metal:pyterpyNO molar ratio of 2 for RE = Y (**9**), Dy (**10**), or Eu (**11**), it was possible to isolate the molecular complexes RE$_4$(tta)$_{12}$(pyterpyNO)$_2$, while using a 5:3 molar ratio, the product La$_5$(tta)$_{12}$(pyterpyNO)$_3$ (**12**) can be obtained. ^{89}Y nuclear magnetic resonance spectroscopy revealed two different yttrium centers at room temperature for **9**. An X-ray diffraction study of **10** showed a symmetrical tetranuclear structure resulting from the coordination of two Dy(tta)$_3$ fragments to the two hypodentate terpyridines of the dinuclear unit and presenting two different coordination sites for metals with coordination numbers of 8 and 9. Magnetic studies of **6** and **10** revealed the presence of an antiferromagnetic interaction between the two Dy(III) atoms bound by the NO bridges. These compounds displayed a slow relaxing magnetization through Orbach (**6**) and Raman (**10**) processes in the absence of an applied magnetic field; the rate increased upon application of a 1 kOe field. **7** and **11** showed a bright red emission typical of Eu^{3+}. The two complexes have similar emission properties mainly determined by the employed β-diketonato ligands.

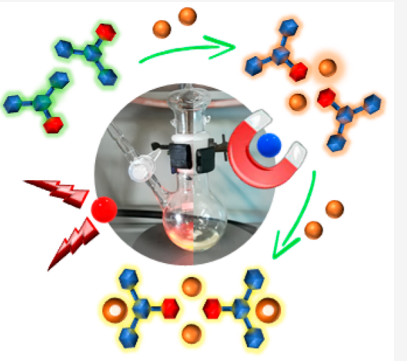

INTRODUCTION

The rational design and synthesis of heterometallic molecular or extended structure compounds rely on suitable connectors showing functional units with different affinities for different metal centers. Several heterometallic d−f coordination polymers (CPs) have been prepared by self-assembly reactions between a mixture of metal ions (usually oxides or nitrates) and organic ligands containing different donor atoms (mostly N and O donors) that can selectively bind to different metal ions. A minor change in the organic linker can induce structural variation of the final coordination structure and of the architecture of new coordination polymers (CPs) and fine control of properties such as gas storage and separation,[1,2] luminescence,[3−5] catalysis,[6,7] and magnetism.[8,9] In particular, organic linkers can efficiently control the spatial organization and the metal−metal distance, a relevant issue in the study of the luminescence or magnetic properties of lanthanide compounds. Multifunctional organic ligands are continuously being examined in the literature, and a full understanding of their coordination chemistry can afford low-nuclearity molecular complexes carrying hypodentate ligands, which can be utilized as building blocks to guarantee better control of the synthesis.[10−15]

Indeed, chemically induced coupling of different molecular units has been shown to be a very powerful tool for the modulation of the magnetic properties of the final adducts. Single-molecule magnets (SMMs) are coordination compounds with a slowly relaxing magnetic moment, arising from a preferential direction of magnetization, with no three-

Received: September 10, 2021
Published: December 14, 2021

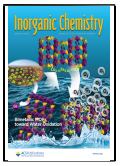

https://doi.org/10.1021/acs.inorgchem.1c02809
Inorg. Chem. 2022, 61, 265−278

dimensional magnetic order.[16,17] Lanthanide ions, due to their largely unquenched orbital moment, giving rise to highly anisotropic paramagnetic ground states, have been widely used for the development of SMMs.[18] One of the most relevant contributions that ditopic organic ligands introduced into the field of molecular magnetism is the possibility of preparing the so-called single-chain magnets (SCMs), one-dimensional coordination polymers featuring significant intrachain magnetic interactions among anisotropic spin bearers but negligible interactions among the different chains, that can present an opening of the magnetic hysteresis loop at cryogenic temperatures.[19] Moreover, the use of divergent organic ligands has been envisaged as promising for the preparation of ordered structures of SMMs with modulable magnetic properties,[20,21] and heterotopic ligands have been used to couple SMM units in one-dimensional[22−24] or three-dimensional[25] coordination polymeric networks. Moving to discrete molecular entities, we found a coordination chemistry bottom-up approach has been used to induce a weak magnetic bias between different paramagnetic centers in SMMs, slowing their dynamics,[26] to prepare polymetallic grids,[27] to increase the number of addressable states in molecular candidates as qbits,[28] or in a molecular switch, allowing movement from two to three available states within a single molecular entity.[29]

With regard to the ligand-sensitized emission of Ln^{3+} ions, most of the literature is focused on (i) discrete systems based on molecular complexes mainly containing only one lanthanide cation and (ii) extended systems such as lanthanide coordination polymers (CPs) and lanthanide metal−organic frameworks (LOFs).

To exploit and tune the emission properties of polynuclear compounds, CPs, and LOFs containing two or more lanthanide ions, the control of the distribution of Ln^{3+} in the different available coordination sites is fundamental. Given the very similar chemistry of the f-block ions, the statistical occupation of the accessible coordination sites is often obtained, thus losing control of the ion−ion interactions as for example in energy transfer processes or ion−ion cross relaxation phenomena.[30,31] These interactions, together with the charge transfer transitions, are often fundamental in determining the emission and functional properties of these compounds and are not trivial to rationalize if the spatial composition (SC)[32−34] is not unequivocally defined. For these reasons, it is necessary to develop synthetic protocols that allow the fine control of SC. In this framework, we decided to follow a stepwise process by using divergent *N*-oxide ligands.

In our previous work, we showed that heterocyclic *N*-oxide ligands such as pyrazine *N*-oxide or 4,4′-bipyridine *N*-oxide (bipyMO) react with neutral lanthanide tris-*β*-diketonato Eu(*β*-diketonate)$_3$ fragments stabilizing homodinuclear molecular compounds Eu_2(*β*-diketonate)$_6$(*N*-oxide)$_y$ (*β*-diketonate = thenoyltrifluoroacetonate, dibenzoylmethanate, benzoyltrifluoroacetonate, or hexafluoroacetylacetonate; y = 2 or 3).[35−37] Heterotopic ligands in these molecular compounds behave as O donor bridging and hypodentate ligands maintaining an uncoordinated nitrogen donor functionality. Luminescence studies have established the effect of the *β*-diketonato and *N*-oxide ligands on the thermometric properties of the obtained compounds, which are determined by the presence of two nonradiative deactivation channels, back energy transfer from Eu^{3+} to the ligand triplet levels and ligand to metal charge transfer (LMCT), the latter being strongly influenced by the *N*-oxide ligands.

Furthermore, self-assembled heterometallic d−f compounds, $[Zn(hfac)_2Eu(hfac)_3(bipyMO)_2]_n$ and $[Co(hfac)_2Dy(hfac)_3(bipyMO)_2]_n$, have been prepared by exploiting the divergent heterotopic 4,4′-bipyridine *N*-oxide ligands. Magnetic and luminescence studies have been carried out on the ordered one-dimensional CPs resulting from a large difference in affinity for the O or N atoms of lanthanide and 3d metal centers.[23] In this context, evaluating how the nature of the rigid heterotopic ligand could influence the identity and the magnetic and luminescence properties of the product of its reaction with neutral lanthanide tris-diketonato fragments Ln(*β*-diketonate)$_3$ appeared to be interesting.

A terpyridyl unit is often used in the design of new organic linkers for the relatively easy synthesis and functionalization, for the strong bond with d transition metals, and for the interesting redox, photoluminescent, and magnetic properties.[38−46] The divergent ligand 4′-(4″′-pyridyl)-2:2′,6′:2″-terpyridine (pyterpy) is well-known in the literature, forming a large number of molecular and extended structure compounds for d metals[47−52] but a limited number of examples for lanthanide metals.[53−55] Furthermore, very little attention has been paid in the literature to the analogue N-oxidated ligand 4′-(4″′-pyridyl-*N*-oxide)-2:2′,6′:2″-terpyridine (pyterpyNO) (Scheme 1); a single paper reported the

Scheme 1. 4′-(4″′-Pyridyl-*N*-oxide)-2:2′,6′:2″-terpyridine (pyterpyNO)

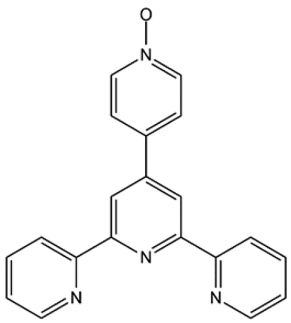

synthesis of a mononuclear iron(II) complex, $[Fe(pyterpyNO)_2](BF_4)_2$, where the metal is coordinated to only the terpyridine unit.[56] Nevertheless, this rigid aromatic ligand with two different binding sites is expected to have a rich coordination chemistry, to be able to control the selective and spontaneous organization of molecular units into ordered structures, and to be potentially useful for the synthesis of heterometallic complexes, a hot topic in the development of polynuclear molecular materials based on lanthanide systems,[57] as previously shown for the analogous 4,4′-bipyridine *N*-oxide ligand.[23,35−37]

In this work, we show that pyterpyNO can bridge two rare-earth centers in a hypodentate mode through the oxygen atom. Careful control of the stoichiometry in the reaction of pyterpyNO with RE(tta)$_3$dme affords complexes with two different molecular compositions, adding new members to the family of polynuclear lanthanide compounds connected through *N*-oxide bridges.[23,35,36] The characterization of the products has been carried out, where appropriate, through nuclear magnetic resonance (NMR), single-crystal X-ray diffraction, magnetic, and photoluminescent studies. Our results introduce the pyterpyNO ligand as a new synthon for the preparation of polynuclear functional materials based on

https://doi.org/10.1021/acs.inorgchem.1c02809
Inorg. Chem. 2022, 61, 265−278

lanthanide ions, whose nuclearity and structure may be controlled in a rational manner.

RESULTS AND DISCUSSION

Dinuclear Complexes. Mononuclear RE(tta)$_3$(dme) [RE = Y (**1**), La (**2**), Dy (**3**), or Eu (**4**); Htta = 1,1,1-trifluoro-3-(2-thenoyl)-acetone; dme = 1,2-dimethoxyethane] precursors have been easily prepared in good yields, following a synthetic route previously reported for Y(hfac)$_3$(dme)[58] (Hhfac = hexafluoroacetylacetone) (see the Supporting Information). Air stable crystalline products, quite soluble in most organic solvents, have been fully characterized. The crystal structures of compounds **3** (Dy) and **4** (Eu) are shown in Figure S1.

pyterpyNO cleanly reacts at room temperature with the diketonato precursor RE(tta)$_3$(dme) in a 1:1 molar ratio (RE = Y, Dy, or Eu), yielding a toluene soluble product. For all compounds, elemental analyses were consistent with the product of a dme substitution reaction, RE(tta)$_3$(pyterpyNO). The infrared (IR) spectra of the recovered products **5** (Y), **6** (Dy), and **7** (Eu) (Figure S2a) are almost completely superimposable, suggesting a similar molecular identity. Suitable crystals for X-ray diffraction have been obtained by slow evaporation of a deuterated chloroform solution of the yttrium compound. A single-crystal diffraction analysis revealed the dinuclear complex Y$_2$(tta)$_6$(pyterpyNO)$_2$·2CDCl$_3$ (**5** CDCl$_3$) in which two pyterpyNO ligands bridge two metal centers through the oxygen atom and the terpyridine fragments are not involved in the metal coordination (Figure 1). The

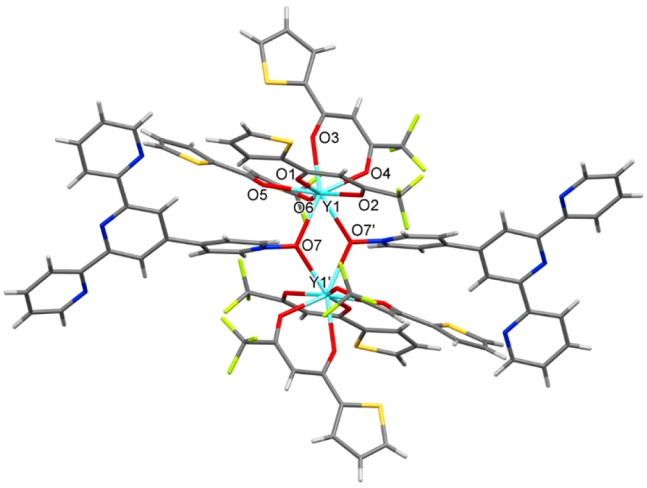

Figure 1. Molecular structure of **5**. Only the most populated positions of the disordered CF$_3$ groups are represented. Prime = 1 − *x*, 1 − *y*, 1 − *z*.

molecule is centrosymmetric, and the coordination around the yttrium atoms is approximately described by a triangular dodecahedron [according to the results obtained with the SHAPE software (reported in Table S2)]. Coordination through an oxygen atom is preferred with respect to the coordination of the terpyridine unit that is expected to be stabilized by a strong chelate effect. Simple steric arguments do not provide a convincing explanation of the outcome, because a coordination number of 9 is common for lanthanides.[59] The hypodentate coordination mode suggests that the oxygen atom of the *N*-oxide moiety is a strong donor for rare-earth centers. Previous findings, with different divergent heterotopic (N and O) ligands (such as 4,4′-bipyridile *N*-oxide or pyrazine *N*-oxide) showing uncoordinated nitrogen atoms in their lanthanide *β*-diketonato complexes, are here confirmed, and a well-defined reactivity is established. Crystals collapse on drying and also on standing in air.

For the diamagnetic yttrium **5**, NMR studies (^{1}H, ^{13}C, ^{19}F, and ^{89}Y NMR) have been carried out (Figure 2a). ^{1}H NMR spectra show a single set of quaterpyridine signals. Significantly, the signal due to the hydrogen close to the terpyridine unit, hydrogen 11 in Figure 2a at 8.79 ppm, is not greatly shifted with respect to the chemical shift of the free ligand at 8.75 ppm, while hydrogen 5, close to the *N*-oxide moiety, moves from 8.35 to 9.34 ppm upon coordination. Fluorine atoms of the tta ligands are all equivalent in the ^{19}F NMR spectra, and a single signal at 31.5 ppm is present in the ^{89}Y NMR spectra, a chemical shift not much different from that found for **1**, 32.8 ppm, that is octacoordinated with all oxygen donors.

La(tta)$_3$(dme) reacted as well with pyterpyNO in toluene at room temperature, although with an important difference with respect to europium, dysprosium, and yttrium analogues. Analytical and spectroscopic (NMR in Figure 2b) data suggest the formation of a dinuclear complex with a [La(tta)$_3$]$_2$(pyterpyNO)$_3$ composition (**8**). As for the yttrium derivative, a single set of pyterpyNO signals is present and a significant shift of hydrogen 5, close to the *N*-oxide moiety, is observed for compound **8**. As opposed to yttrium derivative **5**, in **8** the integral ratio of hydrogen atoms suggests a tta:pyterpyNO molar ratio of 6:3. These results can be rationalized considering that the larger ionic radius of lanthanum ions can afford the presence of three bridging pyterpyNO ligands instead of two as discussed above for yttrium, europium, and dysprosium. Lanthanum complex **8** has three uncoordinated terpyridine units of three hypodentate pyterpyNO ligands. Despite several crystallization attempts, no suitable single crystal has been obtained for an X-ray diffraction study to establish the crystal and molecular structure in the solid state.

Tetra- and Pentanuclear Complexes. pyterpyNO reacts as well with RE(tta)$_3$(dme) (RE = Y, Dy, or Eu) in a 1:2 molar ratio, yielding a single highly soluble complex with a [RE(tta)$_3$]$_4$(pyterpyNO)$_2$ composition [IR (Figure S2b); elemental analysis]. Structural studies of the dysprosium derivative, carried out through X-ray single-crystal diffraction, have confirmed what has been suggested by analytical data: here the heterotopic divergent ligand has a bridging coordination mode. A tetranuclear centrosymmetric molecule with two non-equivalent metals has been identified for [Dy(tta)$_3$]$_4$(pyterpyNO)$_2$ (Figure 3). Two metals in a central position [CN = 8, approximately described by a triangular dodecahedron (see Table S2)] are coordinated by six oxygen atoms of three tta ligands and by two oxygen atoms of two bridging pyterpyNO ligands, while two metals in a lateral position [CN = 9, three-capped trigonal prism (Table S2)] are coordinated by six oxygen atoms of three tta ligands and by three nitrogen atoms of a chelate terpyridine fragment. Crystals collapse on drying and also on standing in air.

NMR characterization has been carried out for RE = Y (Figure 4a). Also in this case, only a single set of quaterpyridine signals is present in the ^{1}H NMR spectrum of **9**, with hydrogen 11 moving from 8.79 to 9.68 ppm as expected for coordination of the terpyridine unit to yttrium and hydrogen 5 only slightly changing its chemical shift. Significantly, two different sets of signals for tta ligands are

https://doi.org/10.1021/acs.inorgchem.1c02809
Inorg. Chem. 2022, 61, 265−278

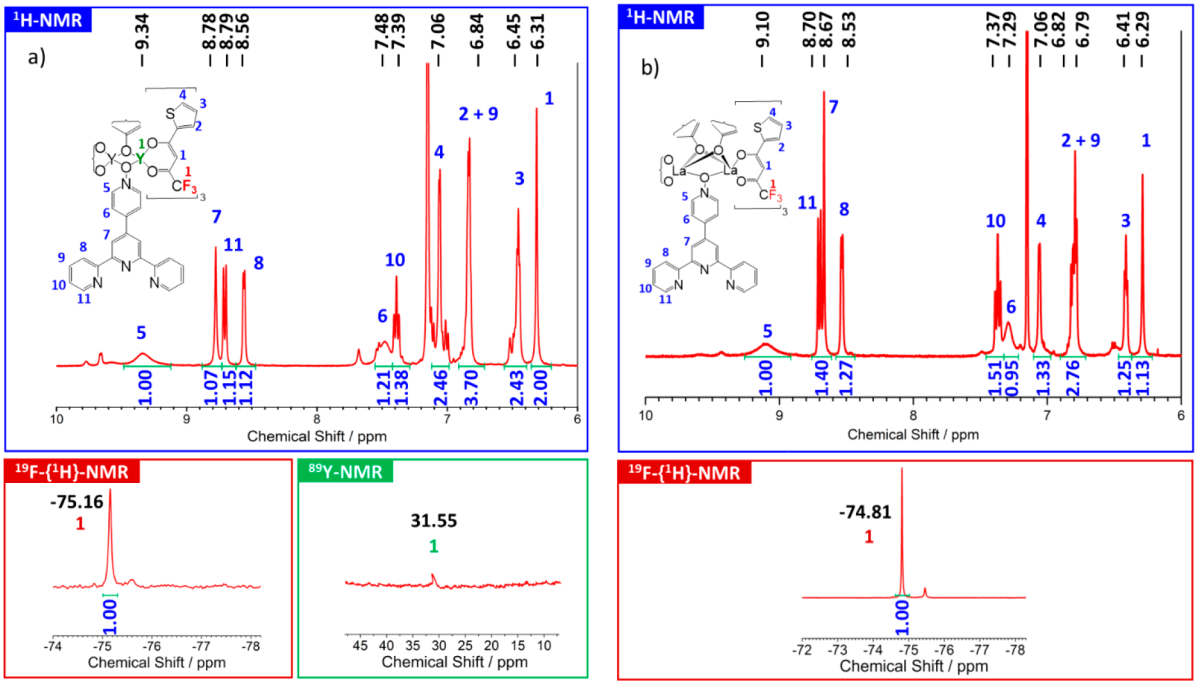

Figure 2. (a) ^{1}H, ^{19}F, and ^{89}Y NMR spectra of **5** and (b) ^{1}H and ^{19}F NMR spectra of **8**.

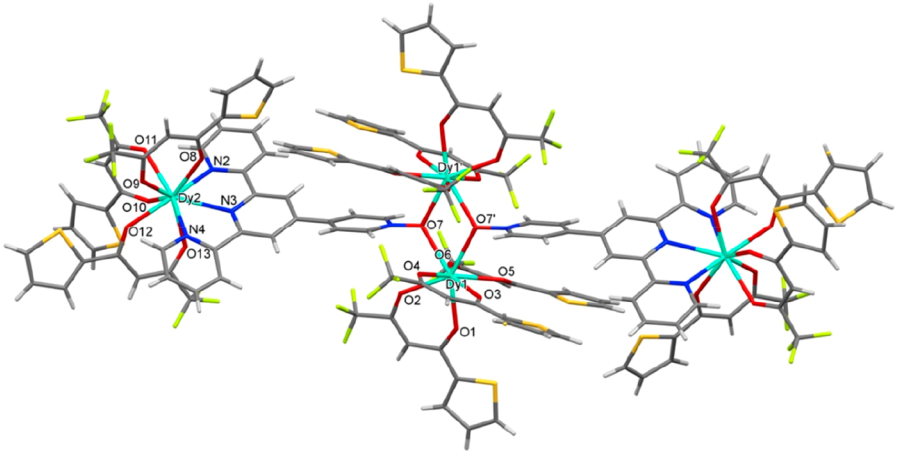

Figure 3. Molecular structure of **10**. Only the more populated positions of the disordered CF_3 groups are represented. Prime = $2 - x$, $1 - y$, $1 - z$.

present in the ^{1}H NMR spectrum, a result that is consistent with two non-equivalent metal centers as revealed by ^{89}Y NMR spectroscopy (signals at 13.9 and 31.4 ppm) and by two different fluorine signals in the ^{19}F NMR spectrum.

$La(tta)_3(dme)$ reacted with pyterpyNO in toluene at room temperature in a 5:3 molar ratio to yield a pentanuclear complex with a $[La(tta)_3]_5(pyterpyNO)_3$ composition (**12**). In Figure 4b, in the ^{1}H NMR spectrum, a significant shift of hydrogen 11, close to the terpyridine moiety, is observed for compound **12**, suggesting the coordination of the terpyridine site of the ditopic ligand. Two different sets of signals due to tta ligands are present in **12** in a 2:3 molar ratio, consistent with ^{19}F NMR spectra in which two fluorine signals are very close to the same molar ratio. Despite several crystallization attempts, no suitable single crystal has been obtained for an X-ray diffraction study to establish the crystal and molecular structure in the solid state.

A toluene solution of $[Y(tta)_3]_2(pyterpyNO)_2$ cleanly and quickly reacts at room temperature with 2 equiv of $Y(tta)_3(dme)$, yielding the tetranuclear compound, so that it is possible to obtain $[Y(tta)_3]_4(pyterpyNO)_2$ both in a single step and upon addition in sequence of 2 equiv of the metal precursor. The synthesis is shown in Figure 5.

Magnetic Study of 6 and 10. *Static Magnetic Properties.* The temperature dependence of the $\chi_M T$ product of compounds **6** and **10** is displayed in Figure 6. For compound **6**, one can see that the experimental room-temperature $\chi_M T$ value (25.92 emu K mol^{-1}) is lower than that expected for the free ion (28.33 emu K mol^{-1}), as frequently found for Dy(III) complexes. This value remains constant when the temperature is decreased to 225 K, where it begins to decrease, according to a crystal field-induced splitting of the $^{6}H_{15/2}$ electronic ground multiplet of the ion,[60] reaching 20.44 emu K mol^{-1} at 5.5 K. At this temperature, there is a change in the slope of the curve, which decreases to 15.36 emu K mol^{-1} at 1.8 K. Because this change in slope cannot be accounted for in terms of magnetic saturation effects, we attribute it to a magnetic exchange between the two Dy(III) ions bridged by the pyterpyNO

https://doi.org/10.1021/acs.inorgchem.1c02809
Inorg. Chem. 2022, 61, 265−278

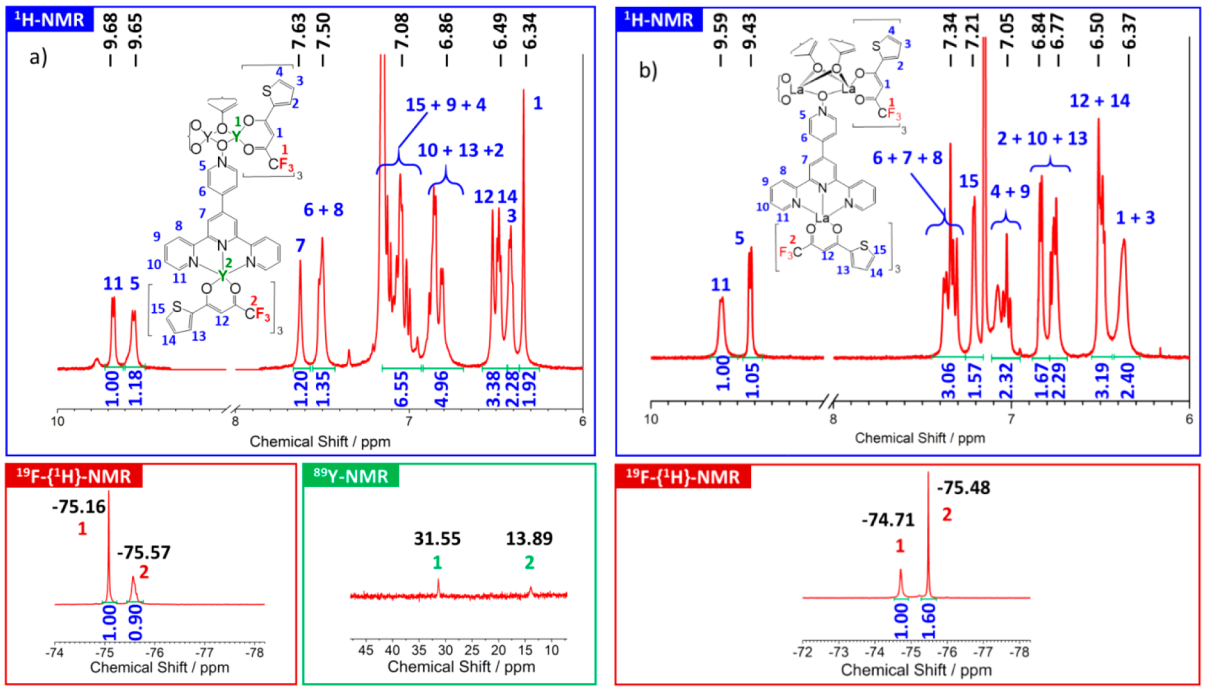

Figure 4. (a) ^{1}H, ^{19}F, and ^{89}Y NMR spectra of **9** and (b) ^{1}H and ^{19}F NMR spectra of **12**.

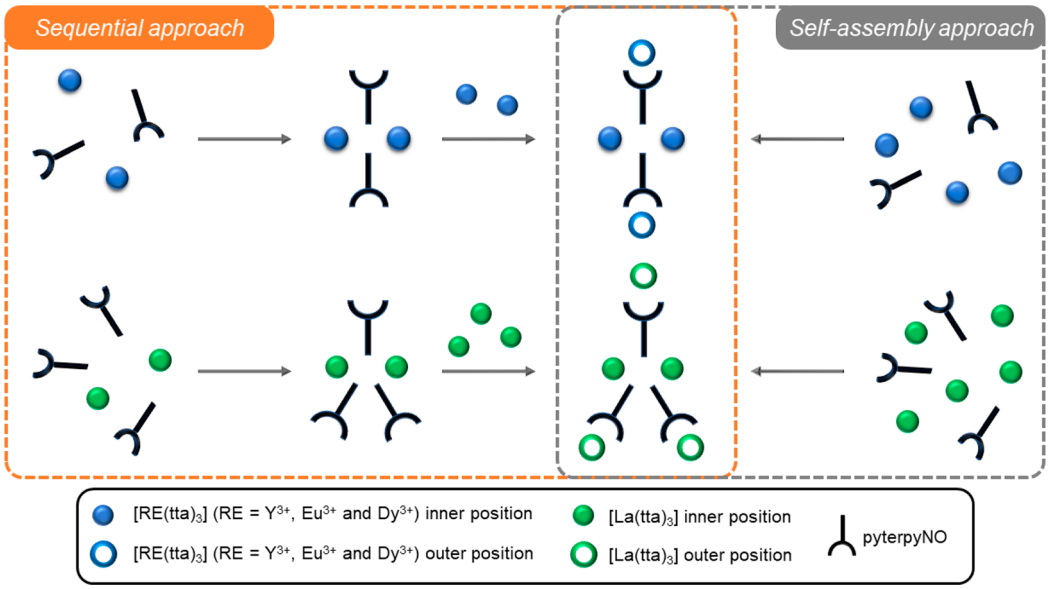

Figure 5. Schematic representation of the assembly of the dinuclear, tetranuclear, and pentanuclear complexes.

ligands. The Dy(III) displays a high magnetic anisotropy at low temperatures, and it is usually modeled as an effective $S = {}^{1}/_{2}$ spin with a theoretical g_z value of 20.[60] A simultaneous fit of the 2−15 K section of this plot and of the isothermal magnetization curves, reported as a red line in Figure 6 and Figure S3, estimates the value of the exchange constant J to be $-1.39(1)$ cm^{-1} ($H = -JS_{1z}S_{2z}$), with a g_z of 18.94(1). Both the sign and the magnitude of the coupling constant are in line with those of similarly oxygen-bridged Dy(III) dimers.[61,62]

As observed for **6**, **10** displays a room-temperature $\chi_M T$ value (50.70 emu K mol^{-1}) that is lower than that expected for four Dy(III) free ions (56.67 emu K mol^{-1}), which decreases upon cooling to reach 35.01 emu K mol^{-1} at 1.8 K. In agreement with the presence of the same dinuclear Dy(III)-bridged core found in **6**, the $\chi_M T$ decreases faster below 6.0 K, suggesting a similar antiferromagnetic interaction to be present in this case, as well. The striking resemblance of the low-temperature part of the $\chi_M T$ product of both compounds is highlighted in the inset of Figure 6. Here, a similar fitting procedure has been performed, considering the presence of two additional, uncoupled, terpyridine-bound Dy(III) ions with Ising-type magnetic anisotropy, yielding a g_z of 18.50(1) for the central Dy(III) ions, a g_z of 18.52(1) for the peripheral Dy(III) ions, and a J of $-1.49(1)$ cm^{-1}. This confirms that for both systems, a weak antiferromagnetic interaction is active between the two Dy(III) ions bound by the *N*-oxide group of the pyterpyNO ligand. The isothermal magnetizations of

https://doi.org/10.1021/acs.inorgchem.1c02809
Inorg. Chem. 2022, 61, 265−278

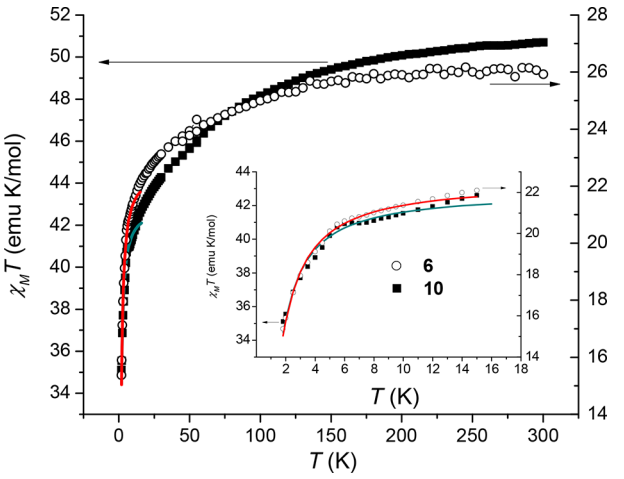

Figure 6. Temperature dependence of the $\chi_M T$ product for compounds **6** and **10**. The lines correspond to the best fitting function, calculated with the model discussed in the text. The inset shows a close-up of the low-temperature region of both curves.

compounds **6** and **10** are reported in Figure S3 and display saturation values of 9.77 and 18.55 μ_B/mol, respectively.

Dynamic Magnetic Properties. The dynamics of the magnetization of compounds **6** and **10** have been assessed with frequency- and temperature-dependent susceptometry. Both systems display slow relaxing magnetization in the absence of an applied static field and, quite interestingly, show an increase in the relaxation rate upon application of a 1 kOe static field. Figure 7 reports the in-phase (χ'_M) and out-of-phase (χ''_M) magnetic susceptibilities of **6**, measured with no applied field. The temperature dependence of the same data is reported as Figure S4. The onset of frequency-dependent peaks in the 5−15 K region is a hint of the slow relaxing magnetization of **6**, and its single-molecule magnet behavior. A careful analysis of the χ''_M plot as a function of field sweeping frequency in the range of 2.0−5.0 K (Figure S5) highlights the presence of two distinct sets of peaks, corresponding to two distinct magnetic relaxation processes. A best fitting procedure of both peaks with the extended Debye model yielded the relaxation times τ reported in Figure 7b. Despite the presence of two Dy(III) ions, the observation of two processes in **6** cannot be attributed to the dinuclear nature of the complex, because the two ions are structurally and magnetically equivalent and should feature a single relaxation process, as reported for other centrosymmetric Dy(III) dinuclear species.[61] We attribute this behavior to the presence of dipolar interactions in the solid state, on the basis of previous reports for Dy(III) systems.[63] The faster process shows almost no temperature dependence, and its average frequency of quantum tunneling of the magnetization (QTM) is estimated to be 12.3 kHz. When the system is heated, the slower process accesses our experimental frequency window and can be fitted using a Raman model and/or an Orbach one, including QTM (see Table S3). Even if both models can fit the experimental data, comparison with the relaxation times measured in a 1 kOe field, for which a fit using a Raman/direct process yields poorer results (*vide infra*), suggests that the actual relaxation mechanism is an Orbach one. It must be pointed out that, for temperatures above 14.5 K, the frequency dependence of the χ''_M plot does not follow the expected bell-shaped curve but

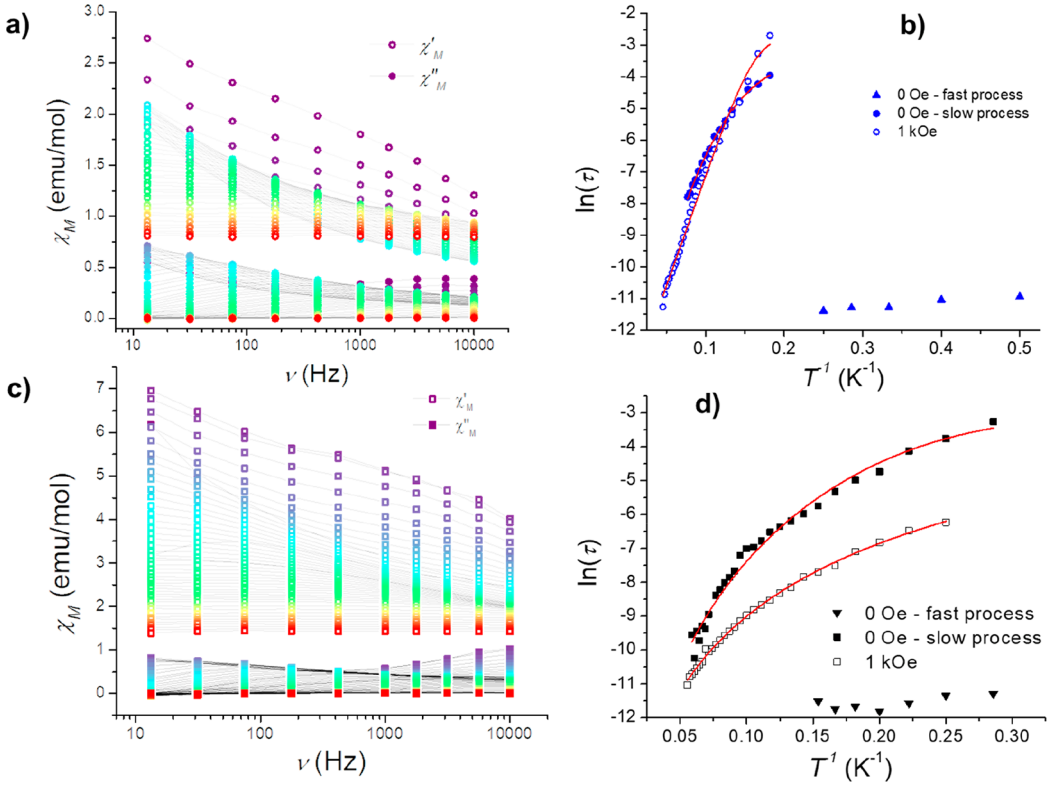

Figure 7. Frequency dependence of the molar in-phase (χ'_M) and out-of-phase (χ''_M) magnetic susceptibilities of compounds (a) **6** and (c) **10**, measured with no static field applied. The temperature dependence of the relaxation times, measured with or without a 1 kOe applied field, is reported as Arrhenius plots in panels b (for **6**) and d (for **10**). The best fitting functions are discussed in the text.

https://doi.org/10.1021/acs.inorgchem.1c02809
Inorg. Chem. 2022, 61, 265−278

becomes wider and cannot be satisfactorily fitted with a single relaxation process, independent of the width of the distribution of the relaxation times. For this reason, an additional peak has been used to reproduce the high-frequency region of the data. However, because the maximum of the curve associated with this second contribution lies outside our frequency window, the uncertainty of the extracted parameters is too large and we did not present them among our results. The complete set of best fitting parameters is reported in Table S3. As previously observed for a structurally related Dy(III) dimer and as one can see in Figure S4, a very tiny dependence of the relaxation dynamics is found upon application of a static magnetic field.[61] Interestingly, the in-field relaxation appears to be slightly faster than the zero-field one for temperatures above 7.5 K. We attribute the observed increase in the relaxation rate with the field to the magnetically induced overcoming of the exchange bias between the two Dy(III) ions in the dimer, as previously observed for other centrosymmetric, antiferromagnetically exchanged Dy(III) dimers.[62] The corresponding Arrhenius plot describes an almost straight line, featuring a slight decrease in slope at low temperatures. In this case, adopting a mixed Raman/direct relaxation model led to a poor fitting of the data, which are however efficiently reproduced by a mixed Orbach/direct mechanism. When compared to the zero-field data, an increase in the effective relaxation barrier [now 70(2) K] and a decrease in τ_0 take place (see Table S3), for which we can account for considering the reduction of the low-temperature quantum pathway of relaxation.

With respect to the Dy(III) core found in compound **6**, it is not surprising that the magnetization dynamics of compound **10** are related to those previously analyzed. At the lowest temperatures and without an applied field, two sets of peaks in the out-of-phase magnetic susceptibility are present in this case, as well. The relaxation rate of the faster process, again, displays a very feeble temperature dependence and can be interpreted as a QTM with an estimated frequency of 17.1 kHz. The increase in the QTM frequency can be tentatively attributed to the increased dipolar field in the solid state by means of the external Dy(III) ions bound to the terpyridine moieties. As opposed to what was found in the case of **6**, the temperature dependence of the slower process in zero field cannot be fitted with an Orbach/QTM model, which cannot reproduce the low-temperature data efficiently. Instead, the relaxation mechanism of **10** without an applied field can be interpreted as a mixed Raman/QTM model [n = 4.5(2) (see Table S4)]. The two peaks could arise from the two structurally inequivalent Dy(III) ions present in the asymmetric unit of the complex, but we believe they can be traced back to the Dy_2 core, as previously seen for compound **6**. With a static applied field of 1 kOe, we find an increase in the relaxation rate, which is similar to that previously observed for **6**. In this case, however, the two Arrhenius plots do not overlap and are better reproduced with a mixed Raman/direct or Raman/QTM mixed relaxation model rather than with an Orbach/direct one, in agreement with zero-field relaxation data (see Table S4 for the parameters). Considering a mixed Raman/QTM approach, a low-n Raman exponent is found [n = 3.25(6)], a behavior previously observed in Dy(III) slow relaxing species, and attributed to the presence of low-lying m_J magnetic states.[64] The observed increase in the tunneling frequency upon application of the static magnetic field has been considered to be the cause of the decrease in the relaxation times and can be attributed to the effect of the magnetic bias that each Dy(III) is exerting on its magnetically coupled, symmetric equivalent, one. This bias has been previously shown to remove the zero-field quantum tunneling pathway of relaxation of the magnetic moment in Dy_2 centrosymmetric systems, shifting it to higher fields.[40]

Photoluminescence Study of 7 and 11. Complexes **7** and **11** belong to the family of polynuclear β-diketonato compounds connected through *N*-oxide ligands that we recently started to study.[35,36] Like the other members of the family, when excited in a wide spectral range that extends from ultraviolet to visible, they show typical red emission, clearly visible to the naked eye, of Eu^{3+}.

The absorption and excitation spectra of **7** and **11** have very similar profiles (Figure 8), but the spectrum of **7** shows a bathochromic shift of ∼10 nm. Because the two complexes have the same ligands, this small difference cannot be ascribed only to ligand-centered transitions. In a previous study, we have shown that the low-energy portions of the absorption spectra of homometallic dimeric complexes, bearing bridging *N*-oxide ligands, have charge transfer character (CT). In these compounds, CT transitions both affect the shape of the absorption spectra and modulate the thermometric properties.[36] By analogy, the differences observed between **7** and **11** are due to low-energy CT transitions.

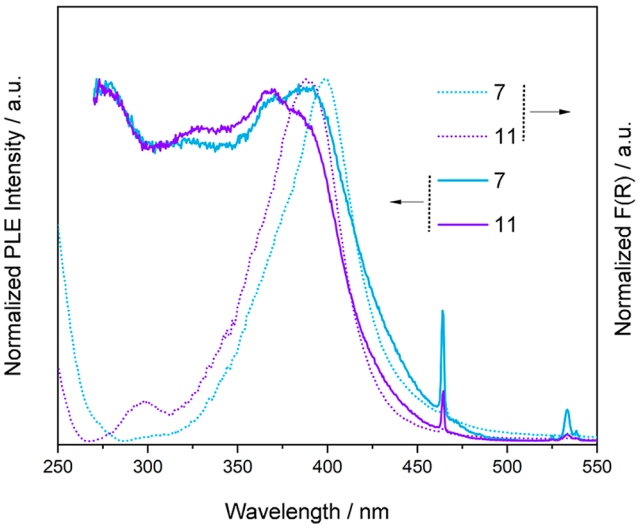

Figure 8. Photoluminescence excitation spectra (PLE, solid lines) and diffuse reflectance absorption spectra (dotted lines) for **7** and **11** monitored on the Eu^{3+} $^5D_0 \rightarrow {}^7F_2$ transition (615 nm).

Luminescence spectra (Figure 9) show only signals from Eu^{3+} 4f−4f intrashell transitions from the $^5D_0$ excited state, populated via the "antenna effect", to the ^7F_J (J = 0, 1, 2, 3, or 4) fundamental multiplet. The tuning of the excitation wavelength across PLE spectra does not affect the number or relative intensity of the different transitions.

While in **7** there are only two equivalent Eu^{3+} ions having coordination numbers of 8; in **11**, other two-Eu^{3+} centers with a CN of 9 are found. The general shape of the spectra is very similar and is predominantly determined by β-diketonato ligands.[35,36] In this type of compound, the symmetry of the Eu^{3+} is very low, as evidenced by the presence of the $^5D_0 \rightarrow {}^7F_0$ transition in the spectra.[65]

Figure 10 shows the high-resolution spectra of **7** and **11** (λ_{exc} = 370 nm), i.e., close to the PLE and absorption maxima for

https://doi.org/10.1021/acs.inorgchem.1c02809
Inorg. Chem. 2022, 61, 265−278

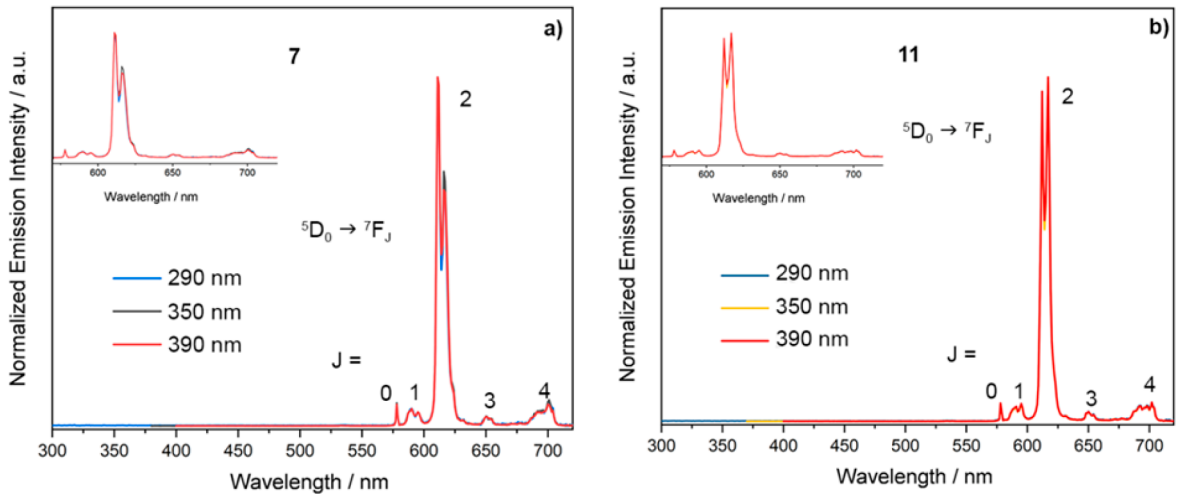

Figure 9. Emission spectra of (a) **7** and (b) **11** obtained by exciting sample powders at different wavelengths. The inset of each panel shows the magnification of the region typical of Eu^{3+} emission.

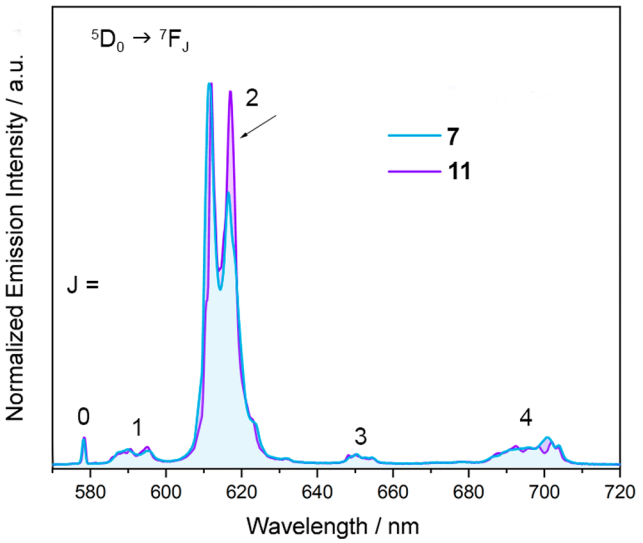

Figure 10. Emission spectra of **7** and **11** (λ_{exc} = 370 nm).

both complexes. The $^5D_0 \rightarrow {}^7F_2$ and $^5D_0 \rightarrow {}^7F_4$ transitions show the most evident differences. In **7**, octacoordinated Eu^{3+} ions display a triangular dodecahedral geometry as in Figure 11 on the left, while when the CN is 9, Ln^{3+} ions have tricapped trigonal prism coordination.

The different coordination geometry affects the shape of the Eu^{3+} emission spectra, and in particular, the crystal field component of the $^5D_0 \rightarrow {}^7F_2$ multiplet at 617 nm, arrowed in the figure, seems to be peculiar for Eu^{3+} having a CN of 9 and, hence, could be used as a sort of fingerprint for these sites.

CONCLUSIONS

The heterotopic divergent pyterpyNO ligand shows a strong preference for the O coordination mode toward rare-earth ions. Complexes having hypodentate terpyridine units, $RE_2(tta)_6(pyterpyNO)_2$ [RE = Y (**5**), Dy (**6**), or Eu (**7**)], can be easily prepared by controlling the stoichiometry of the reaction between pyterpyNO and the air stable diketonato mononuclear metal precursor $RE(tta)_3dme$. For lanthanum, **8**, having a larger ionic radius, three pyterpyNO ligands can bridge two metal ions. Compounds **5**−**8** are expected to have a rich chemistry and to be useful in the mild synthesis of heterometallic complex coordination polymers or metal−organic frameworks. Studies are ongoing in our laboratories.

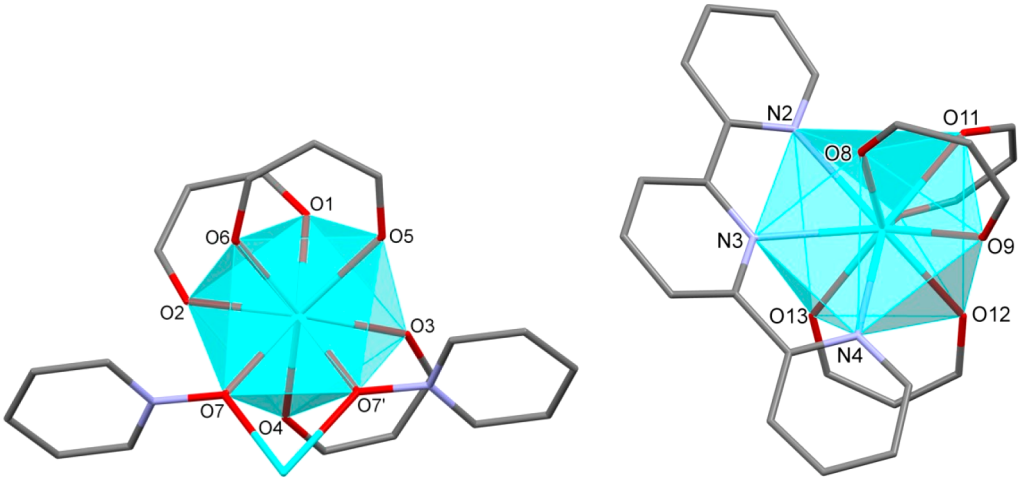

Figure 11. Coordination polyhedra of Dy in **10** for octacoordinated (left) or nonacoordinated ions (right).

https://doi.org/10.1021/acs.inorgchem.1c02809
Inorg. Chem. 2022, 61, 265−278

Reactions with a different stoichiometry [a RE-(tta)$_3$dme:pyterpyNO molar ratio of 2 for RE = Y, Dy, or Eu] afford tetranuclear compounds with the pyterpyNO ligands in a bridging coordination mode and two non-equivalent metal centers for their coordination geometry. Octacoordinated ions in an approximately triangular dodecahedral geometry are only O-coordinated, while nonacoordinated ions in a three-capped trigonal prism geometry have a terpyridine unit in their coordination sphere. Tetranuclear compounds have been obtained not only in a single step but also by addition of a second equivalent of the metal precursor to the dinuclear complexes. This sequential procedure opens the way to the synthesis of heterolanthanide complexes, an issue presently being studied in our laboratories.

From the magnetic point of view, the Dy−O−Dy dinuclear core, present in compounds **6** and **10**, features an antiferromagnetic interaction between the two Dy(III) ions. Such an interaction is weakly sensitive to the presence of two additional Dy(III) ions in the outer terpyridine binding sites, and it is likely to be responsible for the onset of a single-molecular magnet behavior in the absence of an applied static field for both complexes. Quite interestingly, while the relaxation mechanism of **6** can be described as an Orbach one, the temperature dependence of the magnetic relaxation times of **10** cannot be reproduced with this model but is properly fitted with a Raman mechanism. This suggests that the slow relaxing magnetization is related to the central, antiferromagnetically coupled, Dy2 pair. As a confirmation, the relaxation dynamics of compounds **6** and **10** accelerate upon application of a magnetic field, supporting the previous conclusion.

Europium derivatives **7** and **11** displayed a bright red emission that is perceived by the naked eye even when only a few tiny grains of sample powder are subjected to visible or near-ultraviolet light. Emission spectra of **7** and **11** have a similar shape, reflecting the presence of Eu(tta)$_3$ moieties on both octa- and nonacoordinated sites, but the relative intensity of the crystal field component at 612 and 617 nm of the $^5D_0 \rightarrow {}^7F_2$ transition can provide an indication of the occupancy of CN = 9 sites.

EXPERIMENTAL SECTION

Materials and Instrumentation. Anhydrous solvents were purchased from Merck and used as received. 4′-(4-Pyridyl)-2,2′:6′,2″-terpyridine *N*-oxide (pyterpyNO) was synthesized according to the literature.[56] FTIR spectra on solid samples were recorded with a Perkin−Elmer "Spectrum One" spectrometer, equipped with an ATR accessory. ^{1}H, ^{13}C, ^{19}F, and ^{89}Y NMR spectra were recorded with a Bruker "Avance DRX400" spectrometer. Chemical shifts were measured in parts per million (δ) from TMS by residual solvent peaks for ^{1}H and ^{13}C, from $CFCl_3$ for ^{19}F, and from YCl_3 (0.5 M in D_2O) for ^{89}Y. Elemental analysis (C, H, N) was performed at the Dipartimento di Chimica e Chimica Industriale, Università di Pisa.

Absorption spectra of powder samples were recorded using a Cary 5000 UV−vis spectrometer equipped with an integrating sphere. The spectra were normalized and plotted as $F(R)$ versus wavelength. $F(R)$ is the Kubelka−Munk function. A full description can be found elsewhere.[66]

Room-temperature luminescence spectra of sample powders were recorded with a Horiba Jobin Yvon Fluorolog-3 spectrofluorimeter. A full description of the employed setup can be found in a previous paper.[36]

Magnetization Measurements. Samples employed for dc (direct current) and ac (alternating current) measurements consisted of microcrystalline powders of products **6** and **10**, which were wrapped in Teflon tape and pressed as pellets. The dc magnetic characterization was performed on Quantum Design MPMS (Magnetic Properties Measurement System) equipment provided with a 5 T magnet. The dependence of the magnetization (M) on the absolute temperature was investigated between 300 and 45 K using a magnetic field (B) of 1 T and between 45 and 2 K with a field of 0.1 T to prevent magnetic saturation. The magnetic susceptibility per mole (χ_M) was then evaluated as $\chi_M = M_M/B$. Alternating current magnetic susceptibility analyses were performed with a PPMS (Physical Properties Measurement System) platform, also from Quantum Design, with oscillating field frequencies ranging from 10 to 10^4 Hz, and using static magnetic fields of 0 and 1 kOe. The resulting magnetic data were corrected for the diamagnetic contributions of the ligands calculated from Pascal constants,[67] together with those measured for the sample container and the wrapping Teflon tape. The simultaneous fit of the 2−15 K region of the $\chi_M T$ plots and of the isothermal magnetizations of compounds **6** and **10** has been carried out with PHI.[68] For this, each Dy(III) ion has been treated as a purely uniaxial, Ising, $S = {}^1/_2$ effective spin, and the only magnetic interaction assumed to be active is the one between the two Dy(III) ions connected through *N*-oxide bridges. On the basis of the structural properties, only one (two) set of magnetically equivalent Dy(III) ions has been considered for compound **6** (**10**).

The ac susceptibility data were analyzed within the extended Debye model,[69,70] in which a maximum in the out-of-phase component χ''_M of the complex susceptibility is observed when the relaxation time τ equals $(2\pi\nu)^{-1}$. The adopted model includes two different relaxation processes to reproduce a non-zero χ''_M in the low-frequency region of the plots; the corresponding relaxation times extracted from this low-frequency component were, however, not described due to the huge uncertainty associated with them. The frequency dependence of χ''_M at a constant temperature was thus fitted using eq 1:

$$\chi''_M(\omega) = \chi''_{M,LF}(\omega) + \chi''_{M,FIT}(\omega) \quad (1)$$

where each process corresponds to the function reported in eq 2:

$$\chi''_M(\omega) = (\chi_T - \chi_S)[(\omega\tau)^{1-\alpha}\cos(\alpha\pi/2)]/[1 + 2(\omega\tau)^{1-\alpha}\sin(\alpha\pi/2) + (\omega\tau)^{2-2\alpha}] \quad (2)$$

where $\omega = 2\pi\nu$, χ_T and χ_S are the isothermal and adiabatic susceptibilities, i.e., the susceptibilities observed in the two limiting cases, $\nu \rightarrow 0$ and $\nu \rightarrow \infty$, respectively, and α is a parameter that accounts for a distribution of relaxation times.

The temperature dependence of the magnetic relaxation times τ has been fitted using eq 3:

$$\tau^{-1}(T) = \tau_0^{-1}e^{\Delta/kT} + CT^n + BT + QTM \quad (3)$$

where the terms represent Orbach, Raman, direct, and quantum relaxation mechanisms. To avoid overparametrization, in the fitting procedures Raman and Orbach mechanisms have been used alternatively.

Synthesis of RE$_2$(tta)$_6$(pyterpyNO)$_2$, [RE = Y (5), Dy (6), or Eu (7)]. The yttrium case is described at length.

5 *(Y).* pyterpyNO (0.14 g; 0.43 mmol) was added to a solution of Y(tta)$_3$(dme) (0.35 g, 0.42 mmol) in toluene (15 mL) being vigorously stirred. The resulting suspension was mildly heated (70 °C) until the suspended ligand disappeared, and then the solution was cooled to room temperature. Upon addition of heptane (45 mL), a colorless solid precipitated, which was filtered and dried under vacuum for 4 h (0.33 g, 0.15 mmol, 71.9% yield). Anal. Calcd for $Y_2(tta)_6(pyterpyNO)_2$ ($C_{88}H_{52}F_{18}N_8O_{14}S_6Y_2$): C, 49.0; H, 2.4; N, 5.2; S, 8.9. Found: C, 48.7; H, 2.4; N, 4.9; S, 9.1. IR (range of 1700−1100 cm^{-1}): 1624 (m), 1601 (s), 1586 (m), 1538 (s), 1503 (s), 1478 (m), 1441 (w), 1412 (s), 1393 (w), 1357 (m), 1306 (s), 1293 (s), 1244 (m), 1230 (m), 1182 (s), 1127 (s). Slow evaporation of a chloroform solution yielded well-shaped single crystals, suitable for X-ray analysis. ^{1}H NMR (400 MHz, C_6D_6, Scheme 2): δ 9.37 (br s, H^5, 4H), 8.78 (s, H^7, 4H), 8.71 (d, H^{11}, 4H, $^3J_{H11-H10}$ = 7.9 Hz), 8.56 (d, H^8, 4H, $^3J_{H8-H9}$ = 4.3 Hz), 7.50 (br s, H^6, 4H), 7.38 (ddd, H^{10}, 4H,

https://doi.org/10.1021/acs.inorgchem.1c02809
Inorg. Chem. 2022, 61, 265−278

Scheme 2. Numbering for NMR Assignment in 5

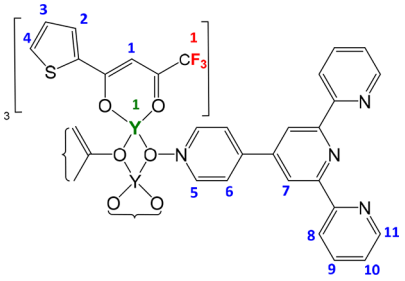

$^3J_{H10-H9}$ = 8.7 Hz, $^3J_{H10-H11}$ = 7.9 Hz, $^4J_{H10-H8}$ = 1.2 Hz), 7.05 (d, H^4, 6H, $^3J_{H4-H3}$ = 3.0 Hz), 6.83 (m, H^2 and H^9, 10H), 6.45 (br s, H^3, 6H), 6.31 (s, H^1, 6H). ^{19}F NMR (400 MHz, C_6D_6): δ −75.1 (s, 18F). ^{13}C NMR (400 MHz, C_6D_6): δ 182.0 (s), 171.1 (q, $^2J_{C-F}$ = 33 Hz), 157.0 (s), 156.0 (s), 149.6 (s), 146.1 (s), 145.5 (s), 136.7 (s), 132.6 (s), 131.4 (s), 130.4 (s), 129.4 (s), 125.7 (s), 124.3 (s), 123.9 (s), 121.4 (s), 120.6 (q, $^1J_{C-F}$ = 286 Hz), 119.7 (s), 92.3 (s). ^{89}Y NMR (400 MHz, C_6D_6): δ 30.5 (s, 2Y).

***6** (Dy).* Starting from 0.16 g of $Dy(tta)_3(dme)$ (0.17 mmol), 0.06 g of pyterpyNO (0.18 mmol), 10 mL of toluene, and 45 mL of heptane, we obtained 0.13 g of $Dy_2(tta)_6(pyterpyNO)_2$ (0.06 mmol, 66.3% yield). IR (range of 1700−1100 cm^{-1}): 1623 (m), 1601 (s), 1587 (m), 1538 (s), 1504 (s), 1471 (m), 1442 (w), 1412 (s), 1393 (w), 1356 (m), 1306 (s), 1292 (s), 1245 (m), 1230 (m), 1183 (s), 1131 (s). Anal. Calcd for $Dy_2(tta)_6(pyterpyNO)_2$ ($C_{88}H_{52}Dy_2F_{18}N_8O_{14}S_6$): C, 45.9; H, 2.3; N, 4.9; S, 8.4. Found: C, 45.6; H, 2.1; N, 4.7; S, 8.5.

***7** (Eu).* Starting from 0.41 g of $Eu(tta)_3(dme)$ (0.45 mmol), 0.15 g of pyterpyNO (0.46 mmol), and 25 mL of toluene, we obtained 0.32 g of $Eu_2(tta)_6(pyterpyNO)_2$ (0.14 mmol, 62.3% yield). IR (range of 1700−1100 cm^{-1}): 1600 (s), 1537 (m), 1502 (m), 1469 (m), 1440 (w), 1412 (m), 1390 (w), 1355 (m), 1301 (s), 1244 (m), 1229 (m), 1182 (s), 1130 (s). Anal. Calcd for $Eu_2(tta)_6(pyterpyNO)_2$ ($C_{88}H_{52}Eu_2F_{18}N_8O_{14}S_6$): C, 46.3; H, 2.3; N, 4.9; S, 8.4. Found: C, 46.0; H, 2.3; N, 4.6; S, 8.6.

$La_2(tta)_6(pyterpyNO)_3$ (8). In a NMR tube, pyterpyNO (12.4 mg, 3.8×10^{-5} mol) and $La(tta)_3(dme)$ (22.7 mg, 2.5×10^{-5} mol) were suspended in anhydrous C_6D_6 (1 mL). When the tube was sonicated and mildly heated, a solution was obtained. NMR data clearly showed that we had produced the desired product. After removal of the volatile phases, a colorless solid was recovered and dried under vacuum for 2 h [18.3 mg of $La_2(tta)_6(pyterpyNO)_3$, 56.7% yield]. IR (range of 1700−1100 cm^{-1}): 1625 (m), 1603 (s), 1586 (m), 1569 (w), 1533 (s), 1500 (s), 1467 (m), 1442 (w), 1412 (s), 1393 (w), 1355 (m), 1291 (s), 1242 (m), 1228 (s), 1180 (s), 1128 (s). Anal. Calcd for $La_2(tta)_6(pyterpyNO)_3$ ($C_{108}H_{66}F_{18}La_2N_{12}O_{15}S_6$): C, 50.2; H, 2.6; N, 6.5; S, 7.5. Found: C, 49.9; H, 2.8; N, 6.3; S, 7.7. ^{1}H NMR (400 MHz, C_6D_6, Scheme 3): δ 9.10 (br s, H^5, 6H), 8.70 (d, H^{11}, 6H,

Scheme 3. Numbering for NMR Assignment in 8

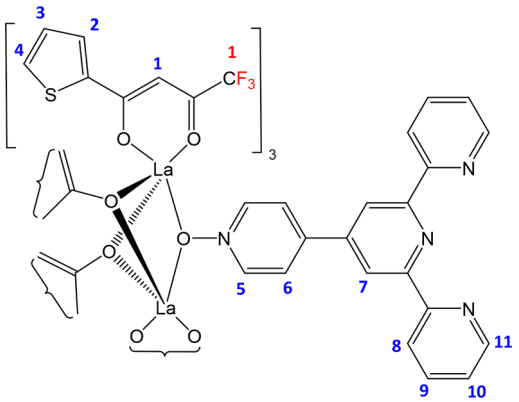

$^3J_{H11-H10}$ = 8.3 Hz), 8.67 (s, H^7, 6H), 8.53 (d, H^8, 6H, $^3J_{H8-H9}$ = 4.2 Hz), 7.37 (ddd, H^{10}, 6H, $^3J_{H10-H11}$ = 8.3 Hz, $^3J_{H10-H9}$ = 6.6 Hz, $^4J_{H10-H8}$ = 1.4 Hz), 7.29 (br s, H^6, 6H), 7.06 (d, H^4, 6H, $^3J_{H4-H3}$ = 2.7 Hz), 6.82 (d, H^2, 6H, $^3J_{H2-H3}$ = 5.1 Hz), 6.79 (t, H^9, 6H, $^3J_{H9-H10}$ = 6.6 Hz, $^3J_{H9-H8}$ = 4.2 Hz), 6.41 (dd, H^3, 6H, $^3J_{H3-H2}$ = 5.1 Hz, $^3J_{H3-H4}$ = 2.7 Hz), 6.29 (s, H^1, 6H). ^{19}F NMR (400 MHz, C_6D_6): δ −74:8 (s, F^1, 18F). ^{13}C NMR (400 MHz, C_6D_6): δ 180.7 (s), 169.7 (q, $^2J_{C-F}$ = 32 Hz), 156.4 (s), 155.7 (s), 149.2 (s), 145.8 (s), 145.4 (s), 141.9 (s), 136.3 (s), 132.7 (s), 131.6 (s), 131.5 (s), 129.3 (s), 123.7 (s), 123.4 (s), 120.9 (s), 120.0 (q, $^1J_{C-F}$ = 287 Hz), 119.0 (s), 91.6 (s).

Synthesis of $RE_4(tta)_{12}(pyterpyNO)_2$ [RE = Y (9), Dy (10), or Eu (11)]. The yttrium case is described at length.

***9** (Y).* In a Schlenk flask, 0.52 g of $Y(tta)_3(dme)$ (0.62 mmol) and 0.10 g of pyterpyNO (0.31 mmol) were dissolved in dce (20 mL). The solution was stirred for 2 days; upon addition of heptane (8 mL), a brown oil precipitated. The solution was therefore evaporated to dryness under vacuum, and we obtained a colorless solid, which was recrystallized with 4 mL of toluene and 4 mL of heptane. This solid was recovered by filtration and dried under vacuum for 8 h. IR (range of 1700−1100 cm^{-1}): 1603 (s), 1580 (w), 1538 (s), 1506 (m), 1475 (w), 1412 (s), 1354 (w), 1305 (s), 1247 (m), 1230 (s), 1183 (s), 1131 (s). When the liquid phase from the filtration was cooled to −20 °C , precipitation of a colorless solid occurred. The latter solid had the same IR spectrum of the former. We recovered overall 0.34 g of $Y_4(tta)_{12}(pyterpyNO)_2$ (0.09 mmol, 59.9% yield). Anal. Calcd for $Y_4(tta)_{12}(pyterpyNO)_2$ ($C_{136}H_{76}F_{36}N_8O_{26}S_{12}Y_4$): C, 44.6; H, 2.1; N, 3.1; S, 10.5. Found: C, 44.2; H, 2.3; N, 2.9; S, 10.7. ^{1}H NMR (400 MHz, C_6D_6, Scheme 4): δ 9.67 (d, H^{11}, 4H, $^3J_{H11-H10}$ = 4.6 Hz), 9.55

Scheme 4. Numbering for NMR Assignment in 9

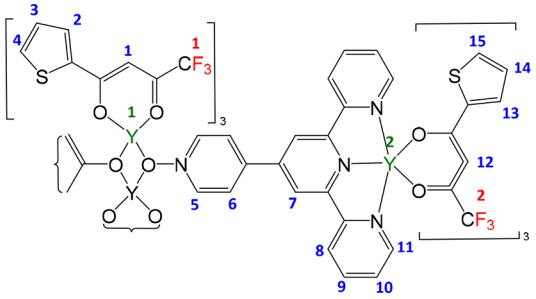

(d, H^5, 4H, $^3J_{H5-H6}$ = 5.7 Hz), 7.63 (s, H^7, 4H), 7.50 (m, H^6 and H^8, 8H), 7.17 (m, H^{15}, 6H), 7.13 (m, H^9, 4H), 7.07 (m, H^4, 6H), 6.88 (d, H^{10}, 4H, $^3J_{H10-H11}$ = 4.6 Hz), 6.85 (d, H^{13}, 6H, $^3J_{H13-H14}$ = 4.4 Hz), 6.81 (d, H^2, 6H, $^3J_{H2-H3}$ = 4.6 Hz), 6.52 (s, H^{12}, 6H), 6.49 (dd, H^{14}, 6H, $^3J_{H14-H15}$ = 5.5 Hz, $^3J_{H14-H13}$ = 4.4 Hz), 6.42 (d, H^3, 6H), 6.34 (s, H^1, 6H). ^{19}F NMR (400 MHz, C_6D_6, Scheme 4): δ −75.1 (s, F^1, 18F), −75.6 (s, F^2, 18F). ^{13}C NMR (400 MHz, C_6D_6): δ 182.2 (s), 181.0 (s), 170.9 (q, $^2J_{C-F}$ = 30 Hz), 170.6 (q, $^2J_{C-F}$ = 31 Hz), 156.1 (s), 153.0 (s), 151.9 (s), 147.4 (s), 146.9 (s), 145.8 (s), 145.4 (s), 144.2 (s), 138.3 (s), 137.9 (s), 132.9 (s), 131.5 (s), 130.7 (s), 129.4 (s), 125.4 (s), 123.8 (s), 121.6 (s), 120.1 (q, 2C, $^1J_{C-F}$ = 286 Hz), 120.0 (s), 118.8 (s), 92.4 (s), 91.8 (s). ^{89}Y NMR (400 MHz, C_6D_6, Scheme 4): δ 31.4 (s, Y^1, 2Y), 13.9 (s, Y^2, 2Y).

***10** (Dy).* pyterpyNO (0.07 g, 0.21 mmol) and $Dy(tta)_3(dme)$ (0.39 g, 0.43 mmol) were dissolved in toluene (10 mL) while being vigorously stirred. The solution was stirred for 2 days, and then upon addition of heptane (40 mL), a colorless solid precipitated. This solid was filtered and dried under vacuum for 8 h. We obtained 0.29 g of $Dy_4(tta)_{12}(pyterpyNO)_2$ (0.07 mmol, 69.8% yield). IR (range of 1700−1100 cm^{-1}): 1604 (s), 1577 (w), 1537 (s), 1504 (m), 1474 (w), 1413 (s), 1354 (w), 1305 (s), 1245 (m), 1229 (s), 1184 (s), 1135 (s). Slow evaporation of a toluene solution yielded well-shaped single crystals, suitable for X-ray analysis. Anal. Calcd for $Dy_4(tta)_{12}(pyterpyNO)_2$ ($C_{136}H_{76}Dy_4F_{36}N_8O_{26}S_{12}$): C, 41.3; H, 1.9; N, 2.8; S, 9.7. Found: C, 41.7; H, 2.1; N, 2.8; S, 9.9.

https://doi.org/10.1021/acs.inorgchem.1c02809
Inorg. Chem. 2022, 61, 265−278

11 (Eu). pyterpyNO (0.09 g, 0.28 mmol) and $Eu(tta)_3(dme)$ (0.51 g, 0.56 mmol) were dissolved in toluene (20 mL) while being vigorously stirred. The solution was stirred for 2 days, and then upon addition of heptane (40 mL), a light yellow solid precipitated. This solid was filtered and dried under vacuum for 8 h. We obtained 0.38 g of $Eu_4(tta)_{12}(pyterpyNO)_2$ (0.10 mmol, 69.2% yield). IR (range of 1700−1100 cm^{-1}): 1600 (s), 1536 (m), 1504 (m), 1471 (m), 1411 (m), 1355 (w), 1298 (s), 1244 (m), 1229 (m), 1181 (m), 1133 (s). Anal. Calcd for $Eu_4(tta)_{12}(pyterpyNO)_2$ ($C_{136}H_{76}Eu_4F_{36}N_8O_{26}S_{12}$): C, 41.7; H, 2.0; N, 2.9; S, 9.8. Found: C, 42.0; H, 2.0; N, 2.9; S, 9.8.

$La_5(tta)_{15}(pyterpyNO)_3$ (12). In a NMR tube, pyterpyNO (6.5 mg, 2.0×10^{-5} mol) and $La(tta)_3(dme)$ (29.2 mg, 3.3×10^{-5} mol) were suspended in anhydrous C_6D_6 (1 mL). When the tube was sonicated and mildly heated, we obtained a solution. ^1H NMR (400 MHz, C_6D_6, Scheme 5): δ 9.59 (br s, H^5, 6H), 9.43 (d, H^{11}, 6H, $^3J_{H11-H10}$ = 4.9 Hz), 7.37 (d, H^6, 6H, $^3J_{H6-H5}$ = 6.0 Hz), 7.34 (s, H^7, 6H), 7.31 (d, H^8, 6H, $^3J_{H8-H9}$ = 8.2 Hz), 7.21 (br s, H^{15}, 9H), from 7.11 to 6.98 (m, H^4 and H^9, 12H), 6.84 (d, H^{13}, 9H, $^3J_{H13-H14}$ = 4.2 Hz), 6.77 (d, H^{10}, 6H, $^3J_{H10-H11}$ = 4.9 Hz), 6.76 (d, H^2, 6H, $^3J_{H2-H3}$ = 5.5 Hz), 6.51 (s, H^{12}, 9H), 6.49 (m, H^{14}, 9H), 6.37 (br s, H^1 and H^3, 12H). ^{19}F NMR (400 MHz, C_6D_6 Scheme 5): δ −74.7 (s, F^1, 18F), −75.5 (s, F^2, 27F).

Scheme 5. Numbering for NMR Assignment in 12

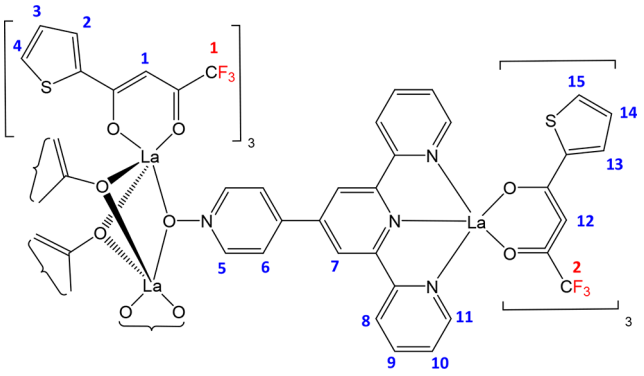

X-ray Diffraction Studies. Crystals of **5** and **10** were selected at room temperature (293 K), sealed in glass capillaries, and analyzed with a Bruker Smart Breeze CCD diffractometer equipped with Mo Kα radiation. The lattice parameters and some collection details are summarized in Table 1. After correction for Lorentz and polarization effects and for absorption, structures were determined with the ShelXT[71] program by intrinsic phasing and refined with the ShelXL[72] package using least-squares minimization.[73] All four structures present disorder in some CF_3 groups, and those of **5** and **10** also in the orientation of thiophene groups, which were refined as being distributed in two limit positions distinguished by different rotations about the C−C bond. The crystal structure of **5** is completed by two molecules of the solvent chloroform for each complex molecule. Some solvent molecules (toluene) are also present in the crystal structure of **10**. Four of them for each complex molecule were localized in the difference Fourier map, but the remaining ones, probably two, could not be located due to the excessive disorder. In this way, a relevant cavity remained in the final structural model. To obtain a model that met CheckCIF's requirements, the localized solvent was removed and the entire contribution of the disordered solvent was subtracted with the SQUEEZE procedure contained in the PLATON program.[74] It is quite relevant to note that the program reports that it has found 551 electrons in the solvent accessible voids, a number quite close to the 600 electrons present in 12 molecules of toluene, six for each molecule of the complex. The final reliability factors for the reported structures are listed in Table 1.

Other control calculations were performed with the programs contained in the WINGX suite.[75] X-ray crystallographic data in CIF format (CCDC 2088701 and 2088703) can be obtained free of charge from the Cambridge Crystallographic Data Center, 12 Union Road, Cambridge CB2 1EZ, UK; fax: + 44 1223 336 033; or email: deposit@ccdc.cam.ac.uk.

■ ASSOCIATED CONTENT

Supporting Information

The Supporting Information is available free of charge at https://pubs.acs.org/doi/10.1021/acs.inorgchem.1c02809.

Table 1. Crystal Data and Refinement Summaries for 5 and 10

	5·2$CDCl_3$	**10** (with solvent)
CCDC number	2088701	2088703
empirical formula	$C_{90}H_{54}Cl_6F_{18}N_8O_{14}S_6Y_2$	$C_{136}H_{76}Dy_4F_{36}N_8O_{26}S_{12}$[+solvent]
formula weight	2396.29	3956.76
crystal system	monoclinic	monoclinic
space group	$C2/c$	$P2_1/n$
a (Å)	23.6382(6)	13.7999(4)
b (Å)	16.0069(4)	38.7002(11)
c (Å)	27.4222(6)	18.5473(6)
β (deg)	101.9140(10)	103.7490(10)
volume (Å^3)	10152.3(4)	9621.5(5)
Z	4	2
ρ_{calc} (g cm^{-1})	1.568	1.366
μ (mm^{-1})	1.516	1.755
$F(000)$	4800	3872
θ range (deg)	1.64−26.5	2.39−26.4
no. of reflections collected	49343	93532
no. of independent reflections	10396	19621
goodness of fit on F^2	1.026	0.894
final R_1 [$I \geq 2\sigma(I)$]	0.0539	0.0406
final wR_2 [$I \geq 2\sigma(I)$]	0.1592	0.1139
final R_1 (all data)	0.0651	0.0586
final wR_2 (all data)	0.1692	0.1271
largest peak, hole (electron Å^{-3})	0.900, −0.963	0.930, −0.606

https://doi.org/10.1021/acs.inorgchem.1c02809
Inorg. Chem. 2022, 61, 265−278

Syntheses of RE(tta)$_3$dme [RE = Y (**1**), La (**2**), Dy (**3**), or Eu (**4**)] crystallographic data for **3** and **4**, and additional magnetic studies (PDF)

Accession Codes

CCDC 2088700−2088703 contain the supplementary crystallographic data for this paper. These data can be obtained free of charge via www.ccdc.cam.ac.uk/data_request/cif, or by emailing data_request@ccdc.cam.ac.uk, or by contacting The Cambridge Crystallographic Data Centre, 12 Union Road, Cambridge CB2 1EZ, UK; fax: +44 1223 336033.

AUTHOR INFORMATION

Corresponding Author

Luca Labella − *Dipartimento di Chimica e Chimica Industriale and CIRCC, Università di Pisa, I-56124 Pisa, Italy; CNR ICMATE and INSTM, Dipartimento di Scienze Chimiche, Università di Padova, I-35131 Padova, Italy;* orcid.org/0000-0001-5001-7853; Email: luca.labella@unipi.it

Authors

Lorenzo Fioravanti − *Dipartimento di Chimica e Chimica Industriale and CIRCC, Università di Pisa, I-56124 Pisa, Italy*

Luca Bellucci − *Dipartimento di Scienze Chimiche and CNR ICMATE and INSTM, Dipartimento di Scienze Chimiche, Università di Padova, I-35131 Padova, Italy*

Lidia Armelao − *Dipartimento di Scienze Chimiche and INSTM, Università di Padova, 1-35131 Padova, Italy; Dipartimento di Scienze Chimiche e Tecnologie dei Materiali (DSCTM), Consiglio Nazionale delle Ricerche, 00185 Roma, Italy*

Gregorio Bottaro − *CNR ICMATE and INSTM, Dipartimento di Scienze Chimiche, Università di Padova, I-35131 Padova, Italy;* orcid.org/0000-0001-6196-8638

Fabio Marchetti − *Dipartimento di Chimica e Chimica Industriale and CIRCC, Università di Pisa, I-56124 Pisa, Italy*

Francesco Pineider − *Dipartimento di Chimica e Chimica Industriale and CIRCC, Università di Pisa, I-56124 Pisa, Italy;* orcid.org/0000-0003-4066-4031

Giordano Poneti − *Instituto de Química, Universidade Federal do Rio de Janeiro, 21941-909 Rio de Janeiro, Brazil;* orcid.org/0000-0002-1712-4611

Simona Samaritani − *Dipartimento di Chimica e Chimica Industriale and CIRCC, Università di Pisa, I-56124 Pisa, Italy;* orcid.org/0000-0002-3518-3164

Complete contact information is available at: https://pubs.acs.org/10.1021/acs.inorgchem.1c02809

Notes

The authors declare no competing financial interest.

ACKNOWLEDGMENTS

The authors thank Dr. Lorenzo Bonaldi for preliminary studies. G.P. gratefully acknowledges FAPERJ for financial support through Grants E-26/202.912/2019, SEI-260003/001167/2020, and E-26/010.000978/2019. F.P. acknowledges Prof. Roberta Sessoli (University of Florence, Florence, Italy) for granting access to the magnetic characterization platforms.

REFERENCES

(1) Zhao, X.-Q.; Zhao, B.; Ma, Y.; Shi, W.; Cheng, P.; Jiang, Z.-H.; Liao, D.-Z.; Yan, S.-P. Lanthanide(III)−Cobalt(II) Heterometallic Coordination Polymers with Radical Adsorption Properties. *Inorg. Chem.* **2007**, *46* (15), 5832−5834.

(2) Farha, O. K.; Spokoyny, A. M.; Mulfort, K. L.; Hawthorne, M. F.; Mirkin, C. A.; Hupp, J. T. Synthesis and Hydrogen Sorption Properties of Carborane Based Metal−Organic Framework Materials. *J. Am. Chem. Soc.* **2007**, *129* (42), 12680−12681.

(3) Ward, M. D. Transition-Metal Sensitised near-Infrared Luminescence from Lanthanides in d−f Heteronuclear Arrays. *Coord. Chem. Rev.* **2007**, *251* (13−14), 1663−1677.

(4) Cui, Y.; Yue, Y.; Qian, G.; Chen, B. Luminescent Functional Metal−Organic Frameworks. *Chem. Rev.* **2012**, *112* (2), 1126−1162.

(5) Pan, M.; Liao, W. M.; Yin, S. Y.; Sun, S. S.; Su, C. Y. Single-Phase White-Light-Emitting and Photoluminescent Color-Tuning Coordination Assemblies. *Chem. Rev.* **2018**, *118* (18), 8889−8935.

(6) Rath, A.; Aceves, E.; Mitome, J.; Liu, J.; Ozkan, U. S.; Shore, S. G. Application of $\{(DMF)_{10}Ln_2[Pd(CN)_4]_3\}_\infty$ (Ln = Yb, Sm) as Lanthanide−Palladium Catalyst Precursors Dispersed on Sol−Gel−TiO_2 in the Reduction of NO by Methane in the Presence of Oxygen. *J. Mol. Catal. A: Chem.* **2001**, *165* (1−2), 103−111.

(7) Shore, S. G.; Ding, E.; Park, C.; Keane, M. A. Vapor Phase Hydrogenation of Phenol over Silica Supported Pd and Pd-Yb Catalysts. *Catal. Commun.* **2002**, *3* (2), 77−84.

(8) Tanase, S.; Reedijk, J. Chemistry and Magnetism of Cyanido-Bridged d−f Assemblies. *Coord. Chem. Rev.* **2006**, *250* (19−20), 2501−2510.

(9) Wang, J.; Feng, M.; Akhtar, M. N.; Tong, M. L. Recent Advance in Heterometallic Nanomagnets Based on TM_xLn_{4-x} Cubane Subunits. *Coord. Chem. Rev.* **2019**, *387*, 129−153.

(10) Niu, Z.; Ma, J.-G.; Shi, W.; Cheng, P. Water Molecule-Driven Reversible Single-Crystal to Single-Crystal Transformation of a Multi-Metallic Coordination Polymer with Controllable Metal Ion Movement. *Chem. Commun.* **2014**, *50*, 1839.

(11) Merkens, C.; Englert, U. Ordered bimetallic coordination networks featuring rare earth and silver cations. *Dalton Trans.* **2012**, *41*, 4664.

(12) Srivastava, S.; Gupta, R. Metalloligands to material: design strategies and network topologies. *CrystEngComm* **2016**, *18*, 9185.

(13) Garibay, S. J.; Stork, J. R.; Cohen, S. M. The Use of Metalloligands in Metal-Organic Frameworks. *Prog. Inorg. Chem.* **2009**, 335−378.

(14) Das, M. C.; Xiang, S.; Zhang, Z.; Chen, B. Metal-Organic Frameworks Functional Mixed Metal-Organic Frameworks with Metalloligands. *Angew. Chem., Int. Ed.* **2011**, *50*, 10510−10520.

(15) Kumar, G.; Gupta, R. Molecularly Designed Architectures-the Metalloligand Way. *Chem. Soc. Rev.* **2013**, *42*, 9403.

(16) Gatteschi, D.; Sessoli, R.; Villain, J. Molecular Nanomagnets. In *Mesoscopic Physics and Nanotechnology Molecular Nanomagnets*; Oxford University Press, 2006; p 395.

(17) Miller, J. S.; Gatteschi, D. Molecule-Based Magnets. *Chem. Soc. Rev.* **2011**, *40* (6), 3065−3066.

(18) Woodruff, D. N.; Winpenny, R. E. P.; Layfield, R. A. Lanthanide Single-Molecule Magnets. *Chem. Rev.* **2013**, *113* (7), 5110−5148.

(19) Caneschi, A.; Gatteschi, D.; Lalioti, N.; Sangregorio, C.; Sessoli, R.; Venturi, G.; Vindigni, A.; Rettori, A.; Pini, M. G.; Novak, M. A. Cobalt(II)-Nitronyl Nitroxide Chains as Molecular Magnetic Nanowires. *Angew. Chem., Int. Ed.* **2001**, *40* (9), 1760−1763.

(20) Jeon, I. R.; Clérac, R. Controlled Association of Single-Molecule Magnets (SMMs) into Coordination Networks: Towards a New Generation of Magnetic Materials. *Dalt. Trans.* **2012**, *41* (32), 9569−9586.

(21) Liu, K.; Zhang, X.; Meng, X.; Shi, W.; Cheng, P.; Powell, A. K. Constraining the Coordination Geometries of Lanthanide Centers and Magnetic Building Blocks in Frameworks: A New Strategy for Molecular Nanomagnets. *Chem. Soc. Rev.* **2016**, *45* (9), 2423−2439.

(22) Rigamonti, L.; Vaccari, M.; Roncaglia, F.; Baschieri, C.; Forni, A. New Silver(I) Coordination Polymer with Fe_4 Single-Molecule Magnets as Long Spacer. *Magnetochemistry* **2018**, *4* (4), 43.
(23) Armelao, L.; Belli Dell'Amico, D.; Bottaro, G.; Bellucci, L.; Labella, L.; Marchetti, F.; Mattei, C. A.; Mian, F.; Pineider, F.; Poneti, G.; Samaritani, S. 1D Hetero-Bimetallic Regularly Alternated 4f-3d Coordination Polymers Based on: N -Oxide-4,4′-Bipyridine (Bipy-MO) as a Linker: Photoluminescence and Magnetic Properties. *Dalt. Trans.* **2018**, *47* (25), 8337−8345.
(24) Bellucci, L.; Labella, L.; Marchetti, F.; Pineider, F.; Poneti, G.; Samaritani, S. Magnetic Relaxation in Dysprosium and Terbium 1D-Zigzag Coordination Chains Having Only 4,4′-Bipyridine as Connector. *Inorg. Chim. Acta* **2021**, *516*, 120165.
(25) Rigamonti, L.; Cotton, C.; Nava, A.; Lang, H.; Rüffer, T.; Perfetti, M.; Sorace, L.; Barra, A. L.; Lan, Y.; Wernsdorfer, W.; Sessoli, R.; Cornia, A. Diamondoid Structure in a Metal−Organic Framework of Fe_4 Single-Molecule Magnets. *Chem. - Eur. J.* **2016**, *22* (38), 13705−13714.
(26) Poneti, G.; Bernot, K.; Bogani, L.; Caneschi, A.; Sessoli, R.; Wernsdorfer, W.; Gatteschi, D. A Rational Approach to the Modulation of the Dynamics of the Magnetisation in a Dysprosium-Nitronyl-Nitroxide Radical Complex. *Chem. Commun.* **2007**, *18*, 1807−1809.
(27) Anwar, M. U.; Thompson, L. K.; Dawe, L. N.; Habib, F.; Murugesu, M. Predictable Self-Assembled [2 × 2] $Ln(III)_4$ Square Grids (Ln = Dy, Tb)—SMM Behaviour in a New Lanthanide Cluster Motif. *Chem. Commun.* **2012**, *48* (38), 4576−4578.
(28) Atzori, M.; Chiesa, A.; Morra, E.; Chiesa, M.; Sorace, L.; Carretta, S.; Sessoli, R. A Two-Qubit Molecular Architecture for Electron-Mediated Nuclear Quantum Simulation. *Chem. Sci.* **2018**, *9* (29), 6183−6192.
(29) Alley, K. G.; Poneti, G.; Robinson, P. S. D.; Nafady, A.; Moubaraki, B.; Aitken, J. B.; Drew, S. C.; Ritchie, C.; Abrahams, B. F.; Hocking, R. K.; Murray, K. S.; Bond, A. M.; Harris, H. H.; Sorace, L.; Boskovic, C. Redox Activity and Two-Step Valence Tautomerism in a Family of Dinuclear Cobalt Complexes with a Spiroconjugated Bis(Dioxolene) Ligand. *J. Am. Chem. Soc.* **2013**, *135* (22), 8304−8323.
(30) Kerbellec, N.; Kustaryono, D.; Haquin, V.; Etienne, M.; Daiguebonne, C.; Guillou, O. An Unprecedented Family of Lanthanide-Containing Coordination Polymers with Highly Tunable Emission Properties. *Inorg. Chem.* **2009**, *48*, 2837−2843.
(31) Tallant, D. R.; Seager, C. H.; Simpson, R. L. Energy Transfer and Relaxation in Europium-Activated Y_2O_3 after Excitation by Ultraviolet Photons. *J. Appl. Phys.* **2002**, *91* (7), 4053−4064.
(32) Osborn Popp, T. M.; Yaghi, O. M. Sequence-Dependent Materials. *Acc. Chem. Res.* **2017**, *50* (3), 532−534.
(33) Bellucci, L.; Bottaro, G.; Labella, L.; Marchetti, F.; Samaritani, S.; Belli Dell'Amico, D.; Armelao, L. Luminescent Sequence-Dependent Materials through a Step by Step Assembly of RE^1-1,4-Benzendicarboxylate-RE^2 (RE^x = Y^{3+}, Eu^{3+} and Tb^{3+}) Architectures on a Silica Surface. *J. Mater. Chem. C* **2019**, *7* (15), 4415−4423.
(34) Bellucci, L.; Bottaro, G.; Labella, L.; Marchetti, F.; Samaritani, S.; Belli Dell'Amico, D.; Armelao, L. 1D-Zigzag Eu^{3+}/Tb^{3+} Coordination Chains as Luminescent Ratiometric Thermometers Endowed with Multicolor Emission. *Materials* **2021**, *14* (21), 6445−6459.
(35) Armelao, L.; Belli Dell'Amico, D.; Bellucci, L.; Bottaro, G.; Ciattini, S.; Labella, L.; Manfroni, G.; Marchetti, F.; Mattei, C. A.; Samaritani, S. Homodinuclear Lanthanide Complexes with the Divergent Heterotopic 4,4′-Bipyridine N -Oxide (BipyMO) Ligand. *Eur. J. Inorg. Chem.* **2018**, *2018* (40), 4421−4428.
(36) Bellucci, L.; Bottaro, G.; Labella, L.; Causin, V.; Marchetti, F.; Samaritani, S.; Belli Dell'Amico, D.; Armelao, L. Composition−thermometric Properties Correlations in Homodinuclear Eu^{3+} Luminescent Complexes. *Inorg. Chem.* **2020**, *59* (24), 18156−18167.
(37) Belli Dell'Amico, D.; Ciattini, S.; Fioravanti, L.; Labella, L.; Marchetti, F.; Mattei, C. A.; Samaritani, S. The Heterotopic Divergent Ligand N-Oxide-4,4′-Bipyridine (BipyMO) as Directing-Agent in the Synthesis of Oligo- or Polynuclear Heterometallic Complexes. *Polyhedron* **2018**, *139*, 107−115.
(38) Wild, A.; Winter, A.; Schlütter, F.; Schubert, U. S. Advances in the Field of π-Conjugated 2,2′:6′,2″-Terpyridines. *Chem. Soc. Rev.* **2011**, *40* (3), 1459−1511.
(39) Housecroft, C. E. Divergent 4,2′:6′,4′′- and 3,2′:6′,3′′-terpyridines as linkers in 2- and 3-dimensional architectures. *CrystEngComm* **2015**, *17*, 7461−7468.
(40) Chandra Mondal, P.; Singh, V.; Zharnikov, M. Nanometric Assembly of Functional Terpyridyl Complexes on Transparent and Conductive Oxide Substrates: Structure, Properties, and Applications. *Acc. Chem. Res.* **2017**, *50* (9), 2128−2138.
(41) Housecroft, C. E.; Constable, E. C. The Terpyridine Isomer Game: From Chelate to Coordination Network Building Block. *Chem. Commun.* **2020**, *56*, 10786.
(42) Constable, E. C.; Housecroft, C. E. 'Simple' Oligopyridine Complexes − Sources of Unexpected Structural Diversity. *Aust. J. Chem.* **2020**, *73* (6), 390−398.
(43) Elahi, S. M.; Raizada, M.; Sahu, P. K.; Konar, S. Terpyridine-Based 3D Metal-Organic-Frameworks:AStructure-Property Correlation Chemistry-A European Journal. *Chem. - Eur. J.* **2021**, *27*, 5858−5870.
(44) Constable, E. C.; Housecroft, C. E. More Hydra than Janus − Non-Classical Coordination Modes in Complexes of Oligopyridine Ligands. *Coord. Chem. Rev.* **2017**, *350*, 84−104.
(45) Habib, F.; Luca, O. R.; Vieru, V.; Shiddiq, M.; Korobkov, I.; Gorelsky, S. I.; Takase, M. K.; Chibotaru, L. F.; Hill, S.; Crabtree, R. H.; Murugesu, M. Influence of the Ligand Field on Slow Magnetization Relaxation versus Spin Crossover in Mononuclear Cobalt Complexes. *Angew. Chem., Int. Ed.* **2013**, *52* (43), 11290−11293.
(46) Goodwin, H. A. Spin Crossover in Cobalt(II) Systems. In *Spin Crossover in Transition Metal Compounds II*; Springer: Berlin, 2004; pp 23−47.
(47) Liu, J.-J.; Lin, Y.-J.; Jin, G.-X. Box-like Heterometallic Macrocycles Derived from Bis-Terpyridine Metalloligands. *Organometallics* **2014**, *33* (5), 1283−1290.
(48) Beves, J. E.; Constable, E. C.; Housecroft, C. E.; Neuburger, M.; Schaffner, S. A One-Dimensional Copper(^{II}) Coordination Polymer Containing $[Fe(Pytpy)_2]^{2+}$ (Pytpy = 4′-(4-Pyridyl)-2,2′:6′,2″-Terpyridine) as an Expanded 4,4′-Bipyridineligand: A Hydrogen-Bonded Network Penetrated by Rod-like Polymers. *CrystEngComm* **2008**, *10* (3), 344−348.
(49) Jacques, A.; Schott, O.; Robeyns, K.; Hanan, G. S.; Elias, B. Hydrogen Photoevolution from a Green-Absorbing Iridium(III)-Cobalt(III) Dyad. *Eur. J. Inorg. Chem.* **2016**, *2016* (12), 1779−1783.
(50) Huang, W.; Wei, H.; Qian, J.; Zhang, C. Ligand-Assisted Conformation of Three Interesting Ni-M (M = Ag, Cu) Heterobimetallic Coordination Polymers: Syntheses, Structures, Thermal and Luminescence Properties. *J. Cluster Sci.* **2016**, *27*, 1655−1669.
(51) Kiskin, M.; Zorina-Tikhonova, E.; Kolotilov, S.; Goloveshkin, A.; Romanenko, G.; Efimov, N.; Eremenko, I. Synthesis, Structure, and Magnetic Properties of a Family of Complexes Containing a $\{Co^{II}_2Dy^{III}\}$ Pivalate Core and a Pentanuclear $Co^{II}_4Dy^{III}$ Derivative. *Eur. J. Inorg. Chem.* **2018**, *2018* (12), 1334−1334.
(52) Hayami, S.; Hashiguchi, K.; Juhász, G.; Ohba, M.; Okawa, H.; Maeda, Y.; Kato, K.; Osaka, K.; Takata, M.; Inoue, K. 1-D Cobalt(II) Spin Transition Compound with Strong Interchain Interaction: $[Co(Pyterpy)Cl_2]$*X. *Inorg. Chem.* **2004**, *43* (14), 4124−4126.
(53) Xie, J.; Shu, H. M.; Hu, H. M.; Han, Z. X.; Shen, S. S.; Yuan, F.; Yang, M. L.; Dong, F. X.; Xue, G. L. Syntheses, Structures, and Luminescence Properties of Lanthanide Coordination Polymers with a Polycarboxylic Terpyridyl Derivative Ligand. *ChemPlusChem* **2014**, *79* (7), 985−994.
(54) Okawara, T.; Feng, J.; Abe, M.; Hisaeda, Y. Aquabis(1,1,1,5,5,5-Hexafluoroacetylacetonato)[4-(4-Pyridyl)-2,2′:6′,2″ - Terpyridine]-Ytterbium(III) Chloride Methanol Monosolvate Monohydrate. *Acta Crystallogr., Sect. E: Struct. Rep. Online* **2012**, *68* (1), m29.

https://doi.org/10.1021/acs.inorgchem.1c02809
Inorg. Chem. 2022, 61, 265−278

(55) Carlson, C. N.; Kuehl, C. J.; Da Re, R. E.; Veauthier, J. M.; Schelter, E. J.; Milligan, A. E.; Scott, B. L.; Bauer, E. D.; Thompson, J. D.; Morris, D. E.; John, K. D. Ytterbocene Charge-Transfer Molecular Wire Complexes. *J. Am. Chem. Soc.* **2006**, *128* (22), 7230−7241.
(56) Pitarch López, J.; Kraus, W.; Reck, G.; Thünemann, A.; Kurth, D. G. Synthesis, Structure and Reactivity of the Homoleptic Iron(II) Complex of the Novel 4′-(4‴-Pyridyl-N-Oxide)-2,2′:6′,2″-Terpyridine Ligand. *Inorg. Chim. Acta* **2005**, *358* (12), 3384−3390.
(57) Buch, C. D.; Hansen, S. H.; Mitcov, D.; Tram, C. M.; Nichol, G. S.; Brechin, E. K.; Piligkos, S. Design of Pure Heterodinuclear Lanthanoid Cryptate Complexes. *Chem. Sci.* **2021**, *12* (20), 6983−6991.
(58) Malandrino, G.; Lo Nigro, R.; Fragalà, I. L.; Benelli, C. Yttrium *β*-Diketonate Glyme MOCVD Precursors: Effects of the Polyether Length on Stabilities, Mass Transport Properties and Coordination Spheres. *Eur. J. Inorg. Chem.* **2004**, 500−509.
(59) Binnemans, K. Rare-Earth *β*-Diketonates. *Handb. Phys. Chem. Rare Earths* **2005**, *225*, 107−272.
(60) Sorace, L.; Gatteschi, D. Electronic Structure and Magnetic Properties of Lanthanide Molecular Complexes. In *Lanthanides and Actinides in Molecular Magnetism*; John Wiley & Sons, Ltd., 2015; pp 1−26.
(61) Yi, X.; Bernot, K.; Pointillart, F.; Poneti, G.; Calvez, G.; Daiguebonne, C.; Guillou, O.; Sessoli, R. A Luminescent and Sublimable Dy III-Based Single-Molecule Magnet. *Chem. - Eur. J.* **2012**, *36*, 11379−11387.
(62) Long, J.; Habib, F.; Lin, P.-H.; Korobkov, I.; Enright, G.; Ungur, L.; Wernsdorfer, W.; Chibotaru, F. L.; Murugesu, M. Single-Molecule Magnet Behavior for an Antiferromagnetically Superexchange-Coupled Dinuclear Dysprosium(III) Complex. *J. Am. Chem. Soc.* **2011**, *133* (14), 5319−5328.
(63) Jeletic, M.; Lin, P.-H.; Le Roy, J. J.; Korobkov, I.; Gorelsky, S. I.; Murugesu, M. An Organometallic Sandwich Lanthanide Single-Ion Magnet with an Unusual Multiple Relaxation Mechanism. *J. Am. Chem. Soc.* **2011**, *133* (48), 19286−19289.
(64) Abragam, A.; Bleaney, B. *Electron Paramagnetic Resonance of Transition Ions*; Oxford University Press: Oxford, U.K., 1970.
(65) Binnemans, K. Interpretation of Europium(III) Spectra. *Coord. Chem. Rev.* **2015**, *295*, 1−45.
(66) De Bellis, J.; Bellucci, L.; Bottaro, G.; Labella, L.; Marchetti, F.; Samaritani, S.; Belli Dell'Amico, D.; Armelao, L. Single-Crystal-to-Single-Crystal Post-Synthetic Modifications of Three-Dimensional LOFs (Ln = Gd, Eu): A Way to Modulate Their Luminescence and Thermometric Properties. *Dalt. Trans.* **2020**, *49* (18), 6030−6042.
(67) Bain, G. A.; Berry, J. F. Diamagnetic Corrections and Pascal's Constants. *J. Chem. Educ.* **2008**, *85* (4), 532−534.
(68) Chilton, N. F.; Anderson, R. P.; Turner, L. D.; Soncini, A.; Murray, K. S. PHI: A Powerful New Program for the Analysis of Anisotropic Monomeric and Exchange-Coupled Polynuclear d- and f-Block Complexes. *J. Comput. Chem.* **2013**, *34* (13), 1164−1175.
(69) Cole, K. S.; Cole, R. H. Dispersion and Absorption in Dielectrics I. Alternating Current Characteristics. *J. Chem. Phys.* **1941**, *9* (4), 341.
(70) Dekker, C.; Arts, A. F. M.; de Wijn, H. W.; van Duyneveldt, A. J.; Mydosh, J. A. Activated Dynamics in a Two-Dimensional Ising Spin Glass: $Rb_2Cu_{(1-x)}Co_xF_4$. *Phys. Rev. B: Condens. Matter Mater. Phys.* **1989**, *40* (16), 11243.
(71) Sheldrick, G. M. SHELXT - Integrated Space-Group and Crystal-Structure Determination. *Acta Crystallogr., Sect. A: Found. Adv.* **2015**, *71* (1), 3−8.
(72) Sheldrick, G. M. Crystal Structure Refinement with SHELXL. *Acta Crystallogr., Sect. C: Struct. Chem.* **2015**, *71*, 3−8.
(73) Sheldrick, G. M. A Short History of SHELX. *Acta Crystallogr., Sect. A: Found. Crystallogr.* **2008**, *64* (1), 112−122.
(74) Spek, A. L. Single-Crystal Structure Validation with the Program PLATON. *J. Appl. Crystallogr.* **2003**, *36*, 7−13.
(75) Farrugia, L. J. WinGX and ORTEP for Windows: An Update. *J. Appl. Crystallogr.* **2012**, *45* (4), 849−854.

https://doi.org/10.1021/acs.inorgchem.1c02809
Inorg. Chem. 2022, 61, 265−278